Correspondence to:

Professor Mark G. Humphrey

Research School of Chemistry

Australian National University

Canberra, ACT 2601, Australia

T: +61 2 61252927

E: Mark.Humphrey@anu.edu.au

Optical Limiting Properties of (Reduced) Graphene Oxide Covalently Functionalized by Coordination Complexes

D.M. Aradhana S. Dissanayake, Marie P. Cifuentes and Mark G. Humphrey

Research School of Chemistry, Australian National University

Canberra, ACT 2601 (Australia)

Abstract

The nonlinear optical (NLO) and optical limiting (OL) properties of graphene oxide (GO), reduced graphene oxide (RGO), and particularly GO/RGO coordination complex hybrids are reviewed. A brief introduction to mechanisms of OL and a summary of the key measurement techniques for determining NLO/OL merit is provided. A summary of synthetic procedures to GO/RGO coordination complex hybrids is included.

Abbreviations

2PA two-photon absorption

3PA three-photon absorption

ESA excited-state absorption

FCA free carrier absorption

G graphene

GO graphene oxide

ISC intersystem crossing

MPA multiphoton absorption

MPc metal phthalocyanine

NLA nonlinear absorption

NLO nonlinear optical

NLR nonlinear refraction

NLS nonlinear scattering

OL optical limiting

Pc phthalocyanine

PET photo-induced electron transfer

RGO reduced graphene oxide

RSA reverse saturable absorption

SA saturable absorption

ZnPc(DG)4 1,8,15,22-tetra-(3-[2-(2-hydroxyl)ethoxy]ethoxy)phthalocyanine zinc

ZnPc(TD)4 1,8,15,22-tetra(3-(5-hydroxyl)pentyloxy)phthalocyanine zinc

Keywords

Porphyrins; phthalocyanines; optical limiting; nonlinear optics; graphene oxide

Contents

1. Introduction

Graphene oxide (GO) is a unique graphene-based material that possesses distinctive structural and electronic properties due to its oxygenated carbon backbone. GO has attracted attention as a versatile, solution-processable multifunctional carbon platform at which a variety of chemical transformations can be effected by modifying the oxygen-containing functional groups. GO exhibits third-order optical nonlinearities and interesting optical limiting (OL) responses that can be tuned by modifying the sp^2 and sp^3 carbon content. Specifically, it can be integrated with other complementary nonlinear optical (NLO) moieties via covalent or non-covalent surface functionalization strategies. The resultant hybrids have shown NLO and OL performance greater than the sum of the individual components or their physical blends.

This review is primarily focused on third-order NLO and OL properties of hybrids consisting of GO which have been covalently functionalized by coordination complexes. A summary of the fundamentals of OL and the third-order NLO effects contributing to OL is followed by a description of the Z-scan technique, the most popular approach to evaluate third-order NLO and OL properties. We then summarize some of the interesting NLO-based studies of GO-based materials, and report on the third-order NLO and OL properties of hybrids consisting of GO covalently functionalized by coordination complexes, concluding with suggestions for future profitable research in this contemporary interdisciplinary field.

2. Optical limiting processes and procedures

2.1. Passive optical limiting (OL)

Over recent years, the proliferation of laser technology in various research and technological fields has led to an extensive use of high-power laser sources operating at different power levels, pulse widths, repetition rates and a variety of wavelengths from the ultraviolet through the visible light spectrum to the infrared, so it is crucial to design appropriate laser protection devices that protect delicate optical sensors, especially the human eye, from accidental or deliberate exposure to detrimental laser sources, while allowing the sensor to operate under ambient light conditions [1-3].

(Insert Figure 1)

Passive manipulation of laser beams (also known as passive optical limiting) is an effective strategy that can be applied to control the intensity or the fluence of laser beams, so as to avoid unacceptable levels of energy density on the sensor (Figure 1). Passive optical limiting relies on intensity- or fluence-dependent third-order or higher-order NLO processes inherent to certain materials. These materials have the ability to control the intensity of the incoming laser in situ in a predetermined and predictable manner via nonlinear absorption, scattering, diffraction or blocking, as a response to the light-induced modifications in the nonlinear medium [1]. Thus, passive manipulation provides irradiance-dependent dynamic laser protection to the sensor by decreasing the output transmittance with increasing incident light intensity without the aid of an ancillary system to trigger the limiting action [2]. Hence, passive OL has great potential for integration into broadband

sensor protection devices known as passive optical limiters, which operate at a wide range of power levels, wavelengths and pulse durations as well as with frequency-agile lasers. Besides controlling the optical fluence, optical limiters can be used in optical switches for pulse shaping, pulse smoothing and pulse compression [4, 5].

An ideal optical limiter shows high linear transmittance for low input intensities up to a certain threshold value known as the clamping threshold (Figure 2). Upon further increase in input laser intensity above the clamping threshold, the optical limiter starts to attenuate the incoming radiation via energy absorption- or energy spreading-type NLO mechanisms as discussed in detail later [6]; thus, the output transmittance starts to clamp at a constant value that depends on factors such as the concentration of the active species, the geometry of the experimental laser set-up, etc. As a result, the amount of radiation reaching the sensor is limited while the sensor is allowed to function optimally under normal light intensities. However, the OL ability of the medium may be lost after exposure to a particular maximum input fluence known as the damage fluence because of laser-induced irreversible optical damage.

(Insert Figure 2)

In designing a practical optical limiter with high OL efficiency, certain primary requirements need to be fulfilled, such as high linear transmittance at low laser intensities, large nonlinear optical susceptibilities, low optical limiting threshold, and high damage threshold, which collectively give a large dynamic range, fast response time, quick recovery, etc. Besides these requirements, some secondary requirements such as low cost,

light weight, ease of processing and robustness (good mechanical and thermal stability) are important [1]. A vast catalogue of NLO materials with different degrees of OL efficiency have been reported to date [2, 7-10]. However, none of the materials have been demonstrated to possess all the requisites for an ideal optical limiter: each candidate material has one or more shortcomings that can override their favorable OL merits. For example, some materials show promising low limiting thresholds, but low damage thresholds narrow their dynamic range; finding suitable NLO materials with extended dynamic ranges to function optimally at high laser intensities is imperative.

The OL ability of a NLO medium originates from a diverse range of intensity- or fluence-dependent third-order or higher-order nonlinear processes such as nonlinear absorption (NLA), nonlinear refraction (NLR), optically-induced nonlinear scattering (NLS), etc., as a consequence of intense light-induced modifications in the material. Most OL media exhibit multiple nonlinear mechanisms with one or more primary mechanisms depending on the laser parameters such as incident laser intensity, wavelength, repetition rate, and laser pulse duration. In designing a sophisticated optical limiter suitable for a wide range of laser parameters, two or more OL mechanisms can be combined together into a single OL platform to improve the overall OL performance via multiple mechanisms of optical limiting. This can be achieved via suitable design strategies such as hybridization, as discussed later. More information on nonlinear processes contributing to passive optical limiting can be found in reference [1]. In the following sections, the most common third-order nonlinear mechanisms of NLA, NLR and NLS are briefly discussed.

2.2. Nonlinear absorption (NLA)

Nonlinear absorptive OL leads to a strong attenuation of the propagating beam as a result of intensity- or fluence-dependent modifications in the nonlinear absorption coefficient of the medium. Several third-order or higher-order nonlinear mechanisms such as two-photon absorption (2PA), multiphoton absorption (MPA), excited-state absorption (ESA), reverse saturable absorption (RSA), free carrier absorption (FCA), etc., are responsible for such energy absorptive OL. 2PA and MPA processes are instantaneous nonlinear processes that depend on the incident light intensity, whereas ESA, RSA, and FCA are related to accumulative nonlinearities that depend on the energy density or the fluence deposited on the sample. In general, the NLA ability of a molecular material strongly depends on the time during which the laser interacts with the medium (or the pulse width of the laser) and the nonlinear absorption cross-section of individual molecules at a certain wavelength. The dynamics of some of the NLA processes of a polyatomic molecule can be explained with a five-electronic-level Jablonski diagram (Figure 3) which involves both singlet (S_0, S_1, S_2) and triplet electronic states (T_1 and T_2). The absorption cross-section for the absorption from S_0 to S_1 is defined as σ_1 and the absorptions from S_1 to S_2 and from T_1 to T_2 are defined as σ_2 and σ_t, respectively.

(Insert Figure 3)

2PA is an instantaneous NLA process in which two photons with identical (or occasionally different) frequencies are simultaneously absorbed, usually from the ground state to a

higher excited state via a virtual intermediate state. 2PA occurs only if the sum of the frequencies of the two photons is close to the resonant frequency of the molecule. The intensity attenuation of a light beam that propagates through a 2PA-dominant material can be given as below, in the Beer-Lambert formalism [7]:

$$dI/dZ = -(\alpha_0 + \beta I)I \quad \ldots\ldots \quad (1)$$

The intensity-dependent absorption coefficient, α(I), is then:

$$\alpha(I) = \alpha_0 + \beta I \quad \ldots\ldots \quad (2)$$

where I is the laser intensity, Z is the beam propagation direction, α_0 is the linear absorption coefficient, and β is the 2PA coefficient which quantitatively characterizes the magnitude of 2PA of a molecular material at the bulk level. β is proportional to the 2PA cross-section (σ_{2PA}) which quantitatively measures the 2PA ability of an individual molecule at a certain wavelength, as given in equation (3):

$$\sigma_{2PA} = (\hbar\omega\beta)/N \ldots\ldots \quad (3)$$

where ħω is the incident photon energy and N is the molecular number density. As can be seen from the above equation, 2PA-based transmission reduction can be manipulated by tuning the incident laser intensity and the magnitude of β (or the 2PA cross-section). For example, materials with large β values can give more efficient 2PA-induced OL with significant clamping of highly intense laser irradiance such as that from ps or shorter laser

pulses. With ns or longer pulses, high pulse energies are required to achieve high light intensities.

Three-photon absorption (3PA) is another interesting NLA process contributing to OL. It exhibits similar characteristics to 2PA. It is a fifth-order nonlinear process in which three photons are simultaneously absorbed via the intermediacy of virtual states. Beam attenuation via the 3PA process can be given as follows in the Beer-Lambert formalism:

$$dI/dZ = -(\alpha_0 + \alpha_3 I^2)I \quad \ldots\ldots \quad (5)$$

where α_3 is the 3PA coefficient.

RSA involves the sequential absorption of two photons via excited-state absorption if the excited-state absorption cross-section is greater than the ground-state absorption cross-section. At low input intensities, transmittance is governed by ground-state absorption, and the first singlet excited state, S_1, starts to be populated. Electrons may then transfer from S_1 to the long-lived first triplet excited state, T_1, via rapid singlet-triplet intersystem crossing (ISC). Electrons at the singlet S_1 or triplet T_1 excited states may be further excited to higher excited states (from S_1 to S_2 via excited singlet-singlet state absorption, or from T_1 to T_2 via excited triplet-triplet state absorption); thus, more molecules are transferred to higher excited states upon an increase in incident laser intensity, and eventually excited-state absorption starts to dominate over ground-state absorption. As a consequence, the overall absorption from the material increases, and the material exhibits ESA-mediated optical limiting under high-power laser irradiation.

The efficiency of excited-state transitions usually depends on the pulse width of the laser. With singlet-singlet transitions, the relaxation from S_2 to S_1 is an ultrafast process. During long pulse durations (such as on the ns time scale), a substantial amount of the population of the singlet excited states decay back to the ground state due to ultrafast relaxation from S_1 to S_0; thus, singlet-singlet transition-mediated OL becomes less efficient in the ns regime. Some NLO media exhibit efficient triplet-triplet excited-state absorption from T_1 to T_2 under ns pulse regimes, due to rapid ISC that occurs faster than the laser pulse width. ISC facilitates an efficient population transfer from S_1 to T_1 and allows the build-up of a substantial triplet population at T_1.

In contrast, in the shorter ps regime, the S_1 population does not get substantially depleted and molecules re-excite to S_2 via rapid singlet-singlet ESA; thus, the five-level model can be simplified to a three-level model which consists of singlet states only. The intensity change in a laser beam propagating through such a three-level medium can be given as in the propagation equation below, by only considering the electronic transitions involving the S_0, S_1 and S_2 states (transitions from the S_2 state to higher excited states are negligible):

$$dI/dZ = -\{\sigma_1 N_0 + N_2(\sigma_2 - \sigma_1)\}I \quad \ldots\ldots \quad (5)$$

where N_1 and N_2 are the number density of molecules in S_0 and S_1, respectively, and N_0 is the number density of total molecules. It is assumed that $N_1 = N_0$ since $N_1 >> N_2$ and the number density of molecules in S_2 is zero, i.e. $N_3 = 0$. Equation (5) can be further simplified to a format similar to that of equation (1) for 2PA:

$$dI/dZ = -(\alpha_0 + \beta_{eff} I)I \quad \ldots\ldots \quad (6)$$

where β_{eff} is the "effective" nonlinear absorption coefficient which is related to the sequential (two-photon) excited-state absorption, and which is thereby related to RSA.

If the excited-state absorption cross-section is smaller than that of the ground state ($\sigma_2 < \sigma_1$), the material behaves as a saturable absorber. At sufficiently high intensities, the excited state is populated at a rate faster than the population relaxation back to the ground state; thus, the ground state population becomes depleted and absorption from the medium decreases with the increase in the laser intensity. Saturable absorption (SA) does not contribute to optical limiting as RSA does, but it can be applied in passive mode locking and in Q-switching of lasers. In some systems, SA switches to RSA with an increase in excitation laser intensity due to the occurrence of other nonlinear process such as 2PA and ESA which become dominant at high excitation intensities. The intensity attenuation of the radiation propagating through such a medium can be given as below (Beer-Lambert formalism) by combining SA and other 2PA and/or ESA components:

$$dI/dZ = -[\{\alpha_0 /(1 + I/I_s)\} + \beta_{eff} I]I \quad \ldots\ldots \quad (7)$$

The intensity-dependent nonlinear absorption coefficient, $\alpha(I)$, can be written as:

$$\alpha(I) = \{\alpha_0 /(1 + I/I_s)\} + \beta_{eff} I \quad \ldots\ldots \quad (8)$$

where α_0 is the unsaturated linear absorption coefficient, I is the input laser intensity, I_s is the intensity at which ground-state absorption is saturated and β_{eff} is the "effective"

nonlinear absorption coefficient which is usually expressed in cm GW^{-1} and which is related to 2PA and/or sequential two-photon excited-state absorption [11].

2.3. Nonlinear refraction (NLR)

Nonlinear refraction-mediated OL originates from laser-induced non-uniform modifications in the nonlinear refractive index of the medium due to instantaneous or accumulative physical mechanisms such as the Kerr effect, molecular reorientation, thermal nonlinear refraction, photorefraction, etc. These spatially inhomogeneous refractive changes influence the propagation of the incident laser beam through the medium and alter the spatial distribution of the transmitted beam. In these cases, the nonlinear refractive medium acts as either a negative lens or a positive lens, depending on the sign of the nonlinear refractive index change, and shows self-limiting action via self-focusing or self-defocusing of the beam translating through it; as a consequence, a significant fraction of the incident intense light is refracted, redirected and redistributed away from the sensor, and the medium thereby provides OL under intense laser irradiances. In comparison to nonlinear absorptive materials, nonlinear refractive materials exhibit a large dynamic range due to this energy-spreading mechanism.

The refractive index of the material can be expressed as:

$$n = n_0 + \Delta n = n_0 + n_2 I \quad \ldots\ldots \quad (9)$$

where n_0 is the linear refractive index, n_2 is the nonlinear refractive index, I is the intensity of the light, and Δn is positive for self-focusing or negative for self-defocusing. In constructing self-focusing or self-defocusing optical limiters, the geometric configuration of the device is crucial for the provision of efficient refractive OL. The incident laser beam is usually focussed onto the nonlinear refractive medium via a converging lens; this ensures the device is active under low input fluences. An aperture (or pinhole) is usually placed in front of the detector collecting the transmitted light from the medium, so as to control the size of the transmitted beam impinging on the detector. At low intensities, the amount of light passing through the aperture is not significantly affected because there is negligible change in the nonlinear refractivity of the medium. However, under high laser irradiances, a large portion of the incident light is blocked as a consequence of significant modification in the refractive index of the medium [1].

2.4. Nonlinear scattering (NLS)

Optically-induced nonlinear scattering results from an intensity-dependent energy transfer from the laser beam to the nonlinear medium, and a subsequent light scattering in such a way that the amount of light transmitted to the sensor is limited [7]. According to Mie

scattering theory, the effective light scattering occurs via the formation of dynamic scattering centers that have a size which is of the order of the incident wavelength. With an increase in the input intensity, the size of the scattering centers (or the magnitude of their absorption cross-sections) increases and thus efficient OL occurs. Scattering-based OL relies on a host liquid matrix because it facilitates efficient thermally-induced scattering by means of the laser-induced formation of solvent microbubbles. Moreover, solvents show reversible recovery under intense laser fluences, whereas solid matrices frequently show irreversible decomposition due to local heating effects. Note that the thermodynamic properties of the solvent, such as surface tension, viscosity, boiling point, etc. [12, 13], and the characteristics of the OL medium, such as particle size [14], geometry [15], bundle size of carbon nanotubes [16], etc., strongly influence the formation of the scattering centers and thereby the scattering efficiency.

Optically-induced light scattering is the dominant OL mechanism in colloidal suspensions of nanomaterials such as nanoparticles [14, 15], carbon nanotubes [16], fullerenes [17], graphene- and graphene oxide-based materials [18], carbon black [19-22], etc. Scattering centers in such colloidal dispersions mainly originate from laser-induced microbubbles and plasma generation in the medium. The light absorption by particles heats up the surrounding host liquid and once the local temperature exceeds the solvent evaporation temperature, vapor microbubbles are generated which act as scattering centers [23]. This process is effective with ns laser pulse excitation because the solvent evaporation typically takes the order of ns. Sublimation due to ionization of the particles generates microplasmas which also scatter the light [21, 24, 25]. In some cases, heating the material may change the local

density. This leads to non-uniform refractive nonlinearities in the solvent around the particles or at the interface between the nanoparticle and the surroundings, contributing to the scattering [26, 27].

2.5. Open- and closed-aperture Z-scan

The Z-scan method is now the standard technique used in characterizing third-order optical nonlinearities which are light intensity- or fluence-dependent. This procedure measures the nonlinear absorptive and nonlinear refractive properties of a medium which are related to the imaginary part ($\chi^{(3)}_{Im}$) and real part ($\chi^{(3)}_{Re}$) of the third-order nonlinear susceptibility [28, 29]. Open-aperture Z-scan provides information on nonlinear absorptive parameters such as the 2PA coefficient, the 2PA cross-sections, the nonlinear absorption coefficient, etc., while the closed-aperture experiment measures changes in the third-order nonlinear refractive index by examining the self-focusing and self-defocusing of the transmitted light.

In the combined open- and closed-aperture Z-scan set-up (which simultaneously measures nonlinear absorptive and nonlinear refractive properties), a spatially-shaped Gaussian laser beam is focused in such a way that the sample experiences an intensity-spatially-varied optical field as it moves along the *Z*-axis towards, through, and beyond the focal point (located at Z = 0) (Figure 4). Beyond the focal point, and after passing through the sample, the beam is split and the resulting beams sent to two detectors: the open-aperture and the closed-aperture detectors. The closed-aperture detector collects the transmitted light

passing through an aperture placed in front of it and measures the refractive index change in the medium over the intensity change. The open-aperture detector collects all of the light directed to it via the beam splitter, and thereby measures the absorption change in the sample against the intensity change. A reference detector measures the laser intensity of the incident reference signal to monitor fluctuations.

(Insert Figure 4)

Figure 5 shows three representative open-aperture absorptive traces (corresponding to (a) SA, (b) 2PA, and (c) RSA) and two representative closed-aperture refractive traces (corresponding to (d) self-defocusing and (e) self-focusing). In calculating the third-order nonlinear parameters, the experimental transmission traces are normalized by dividing by reference values to remove distortions from laser fluctuations, and then fitted with the corresponding theoretical transmittance curves. Nonlinear scattering can be measured by using another photodetector which is usually sited at an angle to the surface of the sample.

(Insert Figure 5)

3. Potential optical limiting materials

As mentioned earlier, the efficiency of the OL process is strongly governed by the intensity-dependent third-order or higher-order optical nonlinearities, which in turn are closely

related to the structure of the nonlinear medium; thus, a detailed understanding of the underlying nonlinear polarization mechanisms and their relationship to the structural characteristics of the material are imperative. Although a diverse range of nonlinear materials with different degrees of OL efficiencies have been synthesized so far, the specific structural requirements to achieve large OL responses by tuning the underlying electronic characteristics are not fully understood. There are many review papers that discuss the various groups of OL materials and their hybrid/composite materials and relevant nonlinear optical mechanisms in detail [1, 2, 7-10]. Here, we briefly outline some of the interesting OL materials to emphasize their diversity.

In general, organic chromophores with extended π-electron assemblies such as conjugated polymers [30-32], organic dyes [33, 34], conjugated macrocycles such as porphyrins and their metalated derivatives [35-37], phthalocyanines and their metalated derivatives [38-42], etc., show considerable potential for OL applications. Large electron polarization in these conjugated systems leads to purely electronic NLO character with fast response times. Furthermore, their wide structural diversity provides a large number of design possibilities ranging from traditional donor-π bridge-acceptor chromophores to multichromophoric conjugated organic polymers. Some inorganic and semiconductor materials and their hybrid materials such as mixed-metal complexes, metal clusters [24, 43, 44], metal nanomaterials (e.g. nanoparticles [45-47], nanorods [48, 49], and nanowires [50]), and semiconductors [51-55] exhibit significant OL.

Organometallic chromophores such as π-conjugated transition metal alkynyl complexes [8, 56-59] or coordination complex chromophores such as transition metal Schiff-base complexes [60-62] are intriguing classes of materials that (in principle) combine the favorable attributes of organic chromophores and metal moieties together into single molecular frameworks; in these cases, the metal centers act as anchor sites to combine a variety of π-conjugated organic fragments into different geometries, ranging from classical 1D dipolar systems through to 2D and 3D multipolar charge distributions such as those that are quadrupolar or octupolar in nature. Low-lying electronic transitions in the UV-Vis region originate from electron density transfer between the metal atom and the organic π-delocalizable framework (metal-to-ligand and ligand-to-metal charge transfer) are one of the signatures of organometallic- and coordination complex-based chromophores; they usually result in a large dipole moment change between the ground state and an excited state, inducing large NLO responses. The structures of these complexes can be tuned via changes in the transition metals, oxidation states, ligand sets, bonding geometries/coordination patterns, etc., to further tailor the NLO and OL properties.

In addition to these NLO-active small molecules, carbon-based nanomaterials with different geometries such as fullerenes (C_{60}, C_{70}, C_{76}, C_{84}, etc.) [63-70], carbon black [19-22], carbon nanotubes [71-76], graphene nanostructures (graphene nanosheets, graphene nanoribbons) [77-80], and graphene oxide based-materials (graphene oxide nanosheets, graphene oxide nanoribbons, reduced graphene oxide nanosheets) [81-89] are also widely recognized as good candidates for NLO/OL applications. Other than the individual materials themselves, hybrid or composite materials of carbon nanotubes [90-98],

fullerenes [99-104] and graphene oxide-based materials [105-108] with organic molecules, organic dyes, metal nanoparticles, polymers, etc., have also emerged as potential OL materials due to synergistic effects between the constituent moieties of the hybrids [56].

None of the materials alone have demonstrated sufficiently efficient OL for practical devices; thus, finding suitable NLO materials with optimized function at high laser intensities is imperative. Considerable research is still required in the pursuit of nonlinear materials that are needed for modulation or combination of photons with control of magnitude and response time. Because this review highlights the NLO and OL properties of GO-based hybrids of coordination complexes, the fundamental properties of GO and RGO and their NLO responses are discussed in the following section.

3.1. Graphene oxide-based materials in optical limiting

Graphene oxide (GO) is the single-sheet oxidized analogue of graphene. It is synthesized via chemical oxidation of multi-layered graphite followed by solvent exfoliation. During chemical oxidation, random oxidative unzipping and cleavage of the graphene sheets results in a highly heterogeneous oxygenated carbon backbone covalently decorated with randomly distributed multiple oxygen-containing functional groups in various proportions, either on the GO basal plane or at the sheet peripheries (Figure 6a). Recent studies have shown that hydroxyl and epoxy groups are the dominant functional groups on the basal

plane while carboxylic, carbonyl, lactol, etc., groups are located at the sheet edges as the minor oxygenated functional groups [109-111]. These surface oxygenated functional groups play a pivotal role in improving the ease of dispersion and processing of the carbon backbone in various polar solvents and polymer matrices; by exploiting these properties, well-exfoliated colloidal suspensions of mono- and few-layered GO can be easily prepared [112] and can be uniformly deposited onto solid substrates as thin films [83, 113].

(Insert Figure 6)

Upon oxidation, the extended sp^2-conjugated honeycomb lattice of graphene gradually transforms to a highly inhomogeneous carbon backbone comprising a mixture of sp^2- and sp^3-carbon regions in which non-oxidized graphene-like sp^2-hybridized aromatic regions that are a few nm in dimensions are randomly distributed within a highly oxidized sp^3-carbon matrix [109, 114]. Because the fractions of sp^2- and sp^3-carbons and their relative distributions strongly depend on the precursor graphite, the oxidation conditions and the post-work-up conditions, considerable batch-to-batch variations in sheet size, thickness, surface chemistry, defect concentration and distribution, coverage of oxygen functionalities, etc., are inevitable, and these variations (understandably) affect the performance of the final product. Due to this complex nonstoichiometric carbon skeleton possessing randomly distributed oxygen functionalities and other structural defects, it is extremely challenging to develop a structural model that adequately describes the fundamental structure and bonding in GO at the atomic scale. The lack of precise analytical techniques to identify and quantify the various functional groups and their distribution has

further hindered the exploitation of the structure. To date, there have been many conceptual models proposed to depict the molecular structure of GO [115-118], but none have been able to define a precise molecular model although GO has now been subjected to theoretical and experimental studies for many years [119].

GO is an electronically insulating material consisting of conducting π states from sp^2-carbon clusters and a large energy gap between the π states of the sp^3-bonded carbons [120, 121]. Following oxidation of graphene, the π-carrier concentration and the number of conductive pathways along the sheets are significantly reduced, opening up a large energy gap that depends on the level of oxidation; thus, the electrical conductivity of GO is reduced by several orders of magnitude in comparison to that of the precursor semiconducting graphene which possesses a zero-energy band gap. Different local-energy gaps can be distributed across the GO sheet due to the multiple graphene-like sp^2 clusters in the oxidized sp^3-carbon matrix [120]; a wide energy-gap distribution can therefore be anticipated across the GO sheet, depending on the size of the sp^2-hybridized cluster, the relative fraction of the sp^2 clusters, and the distribution of the sp^2 clusters in the sheet [120, 122]. These multiple sp^2- and sp^3-hybridized regions give rise to tuneable optoelectronic properties such as different/multiple NLA processes for different input laser intensities, fluorescence over a broad range of wavelengths, etc., which can be modified by varying the sp^2- and sp^3-carbon fractions [82, 120]. More details of the chemistry of GO including its synthesis, structure and reactivity can be found in recent review papers [110, 119, 123-126].

Although chemical oxidation improves the solubility and the ease of processing of hydrophobic graphene, GO cannot be used as a conductive nanocarbon platform for electric and optoelectronic applications without restoring the lost electrical conductivity via reduction chemistry. GO can be chemically [127-129] or thermally [110, 130] reduced to its reduced form (known as reduced graphene oxide, RGO: Figure 6b) by manipulating the sp^2- and sp^3-carbon fractions via the controlled removal of the oxygen functionalities. Upon reduction, the majority of the oxygen functionalities are removed and the π-conjugation is significantly restored in the form of newly formed sp^2-bonded aromatic regions [130-132]; electronically insulating GO is thereby converted to a semiconducting material and then further to a graphene-like semi-metal, depending on the degree of reduction [121, 130]. During the initial stage of reduction, the carrier transport between the original sp^2-clusters increases via hopping and tunnelling, but upon further reduction, conductive pathways across the sheet are substantially improved; this results from the expanded connectivity among the original sp^2 clusters through the newly formed smaller sp^2 domains that result from deoxygenation [130]. However, the electronic characteristics of RGO do not reach the level of pristine graphene obtained by mechanical cleaving of graphite. This is because the residual oxygen functionalities and other structural imperfections such as Stone-Wales defects, extended topological defects such as clustered carbon pentagons, heptagons, rotated hexagons, and holes strongly disrupt the sp^2 conjugation [109, 133]. It is not possible to remove all of the oxygen functionalities and repair all of the defects formed during both the oxidation or reduction via post-defect healing strategies, and so it is not possible to fully restore the π-conjugation of a highly oxygenated and highly defective GO sheet [134]. The structure and properties of RGO may vary greatly from or closely resemble

pristine graphene, depending on the treatment. RGO can therefore be considered as a conceptually different material from graphene due to the topological defects and residual oxygen functionalities in the extended carbon network, and the fact it does not show fundamental 2D condensed-matter effects such as the quantum Hall effect, etc., inherent to pristine graphene. Moreover, RGO is more adaptable for solvent-based chemical modifications than hydrophobic graphene, due to the remnant surface oxygen functional groups [110, 127-129]. Further details can be found in several comprehensive reviews on the chemistry of RGO [134, 135].

In summary, chemical oxidation followed by reduction can be used as an effective top-down synthetic strategy to produce graphene-like materials that can be solution-processed and that can be available in scalable quantities starting from the inexpensive precursor 3D graphite. Both GO and RGO are versatile, solution-processable precursor carbon platforms that can be used for the fabrication of novel hybrid or composite materials via different covalent and non-covalent functionalization strategies, as discussed in detail below. In the next section, a brief overview of the third-order optical nonlinearities of GO and RGO is presented in order to highlight the potential of these materials as versatile broadband NLO carbon platforms to construct multifunctional OL hybrid systems.

3.2. Nonlinear optical and optical limiting properties of GO and RGO

GO-based materials (both GO and RGO) have received considerable attention for potential OL applications because their NLO behavior can be modified by manipulating the sp^2- and sp^3-carbon fractions in their backbone [82]. A large number of studies have demonstrated nonlinear responses originating from exfoliated sheets of GO/RGO in different aqueous and organic solvents under different excitation conditions (such as different wavelengths and different pulse lengths ranging from fs through ps to ns in duration) [81, 136]. Some studies have examined the NLO and OL responses of exfoliated sheets in host solid matrices such as polymers [137, 138], methyltriethoxysilane-modified silicate glass matrices [84], and thin films deposited on plastic/glass surfaces [83].

GO-based materials exhibit multiple NLA processes simultaneously, such as SA, 2PA, RSA, etc., across different absorption domains, and these collectively give rise to broadband NLO responses in the bulk material that depend on the input excitation intensity. For example, GO/RGO usually show SA-dominated NLA originating from sp^2 cluster sites at low input intensities, and this changes to 2PA-/RSA-dominated OL as the excitation intensity increases due to the contribution of the sp^3-carbon matrix [82, 83, 85, 136]. Moreover, the NLA responses of GO/RGO are strongly affected by the laser pulse duration. For example, GO exhibits SA at low input intensities for both ps and ns pulses at 532 nm, but with an increase in input laser intensity, 2PA dominates the NLA process for ps pulses, while for ns pulses, ESA plays a significant role [136].

The third-order optical nonlinearities of GO can be tuned by manipulating the size, location and the fractions of the sp^2 and sp^3 regions via synthetic strategies [82]. The degree of

oxidation has a strong influence on the magnitude of the NLA responses of GO-based materials [86, 87, 139, 140]. For example, the NLA responses of aqueous suspensions of GO to 532 nm or 1034 nm, ns or ps laser excitation strongly depend on the degree of oxidation [87]. GO with a lower degree of oxidation has larger NLA activity for both visible and infrared excitations, while partially reduced GO samples generated by UV laser irradiation exhibit larger NLA than oxidized GO samples due to the extended π-conjugation. Consistent with these observations, the 2PA coefficients of GO samples for visible or infrared, ps or ns laser excitation decrease with an increase in the degree of oxidation, with the largest values reported for reduced samples and visible ns excitation. These observations are in agreement with significantly superior NLO and better OL efficiency found for few-layer GO compared to single-sheet GO in various organic solvents (532 and 1064 nm wavelength ns laser pulses) [86, 140]; the enhancement is due to increased RSA and/or 2PA resulting from the comparatively larger fraction of localized sp^2 clusters in stacked few-layer GO compared to single-sheet GO. The SA exhibited by single- and few-layer GO suspensions decreases with an increase in the extent of oxidation when measured using fs pulses at 800 nm [82]. With an increase in the input intensity, comparatively highly oxidized GO samples show 2PA-dominated OL behaviour while less oxidized GO displays SA behaviour. These observations suggest control of oxidation as a strategy to manipulate NLA processes such as SA in the sp^2 clusters and 2PA in the sp^3 domains.

Based on the foregoing observations, reduction of the GO backbone (and thereby restoration of the sp^2 conjugation) is, not surprisingly, an effective strategy to improve the

NLO and OL responses. RGO exhibits stronger NLO and OL properties than its precursor GO with the magnitude of the NLO/OL effects depending on the degree of reduction [78, 83, 141]. The NLO and OL properties of GO can be tuned by the controlled reduction of GO thin films deposited on glass and plastic substrates; the reduction can be effected by laser irradiation and exposure to hydrazine vapour for different periods of time, with the modulation of the NLO properties being assessed at 400 nm and 800 nm employing fs laser pulses [83]. The OL responses of GO films are dominated by 2PA/3PA and NLS and are strongly enhanced following partial reduction. Highly reduced GO films obtained by hydrazine exposure show strong SA responses, while the 2PA coefficient of GO is enhanced up to nineteen times at 400 nm and the 2PA and 3PA coefficients of GO at 800 nm are enhanced by twelve and ca. fifteen times, respectively, following laser-induced reduction. The increased optical nonlinearities of the GO films following the initial reduction are linked to the large increase in the localized sp^2 domains. Upon further reduction, and with a low laser fluence (0.6 mJ cm^{-2}), the increase in the sp^2-carbon network through the sp^2 domains results in SA.

An amorphous structural carbon model has been applied to explain the origin of the multiple NLA processes in GO/RGO and the ability to tune NLA by manipulating the sp^2- and sp^3-carbon fraction [85]. According to the model, the GO structure consists of randomly distributed sp^2 cluster islands in a sp^3-carbon matrix as a result of oxidation of the precursor graphite. Upon reduction, small sp^2 domains consisting of irregular carbon conjugates are formed, and they grow in size and in number while the original sp^2 cluster size remains the same. RGO therefore contains three distinct carbon regions: aromatic sp^2 clusters (band gap

ca. 0.5 eV), smaller sp^2 domains resulting from reduction (for which the band gap may vary with domain size - it typically ranges from 0.5 eV to 6 eV), and an amorphous sp^3-carbon matrix (large band gap ca. 6 eV) (Figure 7). SA is associated with the sp^2 clusters and/or sp^2 domains at low input power while 2PA and MPA may originate from the sp^2 domains and the sp^3 carbon matrix at high input power.

(Insert Figure 7)

In addition to NLA- and NLS-derived OL, nonlinear refractive effects have been reported in several studies [88, 142]. Negative NLR has been observed in GO dispersions in DMF in the ns, ps and fs time regimes, while the NLA behaviour changes from SA to RSA with an increase in laser intensity [142]. The NLA and NLR responses of GO thin films deposited on a glass surface and continuously exposed to laser irradiance (800 nm, fs pulses) have been probed until optical breakdown of the material [88]; with an increase in laser input intensity, the initial SA response transforms to an OL response due to MPA-dominated NLA while the NLR behaviour changes from self-focusing (positive nonlinear refractive index) to self-defocusing (negative nonlinear refractive index) via four different stages of nonlinear activity, due to the laser-induced in situ reduction of the GO film. The modifications in the NLA and NLR behaviour correlate with the laser-induced modification of the sp^2/sp^3 carbon ratio. Overall, the experimental studies detailed in this section suggest that mono- or several-layer GO or RGO are potential OL materials with a diverse range of third-order NLO properties originating from their heterogeneous carbon structures, and that their optical nonlinearities can be tuned by varying extents of oxidation or reduction.

3.3. Syntheses and OL studies of (R)GO covalently functionalized by coordination complexes

3.3.1. Surface functionalization of GO

There has been tremendous recent interest in engineering novel GO-based molecular materials and, to that end, a variety of different synthetic strategies have been assayed to functionalize GO and RGO. Surface functionalization is one such design strategy which effectively exploits the heterogeneous surface chemistry of GO-based carbon platforms with complementary functionality of molecules to afford multifunctional hybrid architectures. In the case of GO/RGO, the 2D chemically tuneable surface with large lateral dimensions serves as an ideal carbon platform to construct tailor-made hybrid materials via a range of covalent and non-covalent surface functionalization procedures [123, 126, 143]. The bulk performance of such hybrid materials strongly depends on the nature of the interfacial binding interactions and the degree of functionalization per unit area of the carbon surface; thus, by rationally designing the hybrid, the advantages of both moieties can in principle be harnessed at their full potential [126, 143, 144]. Surface functionalization of GO/RGO is still little explored, but it does possess promise for the synthetic manipulation of the performance of graphitic materials.

GO-based hybrids can exhibit enhanced (or novel) optoelectronic and physicochemical properties at the bulk level that cannot be derived from the individual functional

components or their physical blends [120, 144]. For example, surface functionalization allows the integration of the heterogeneous NLO properties of GO-based carbon platforms with those of complementary NLO chromophores to give a single hybrid architecture, with larger third-order optical nonlinearities and OL responses being possible from the resultant hybrid systems than are available from the individual components [145]. Some nanohybrids have possible biomedical applications such as in bio-sensing and bio-imaging, drug delivery, photo-thermal therapy in cancer treatment, etc. More details on the different covalent and non-covalent functionalization strategies at GO-based substrates and the potential applications of GO-based hybrid materials can be found in review papers [123, 124, 126, 143, 144, 146, 147].

In covalent functionalization, oxygen-containing functional groups at the surface act as anchor sites to bind targeted species via a broad range of functionalization approaches. Amidation and esterification are two commonly used synthetic procedures in which carboxylic groups at the GO surface are employed in anchoring. Certain species can also be directly grafted onto the sp^2 conjugated regions of the RGO surface via reactive intermediates such as aryl diazonium radicals or nitrenes, with a change from the trigonal-planar sp^2 geometry to a tetrahedral sp^3 geometry. A wide range of functional species have been covalently attached to GO or RGO surfaces in this fashion, including porphyrins, phthalocyanines, and their metalated derivatives, C_{60}, carbon nanotubes, polythiophenes or oligothiophenes [100, 148], polymers [94, 106], metal nanoparticles [149], coordination complexes and organometallics [144], etc.

The GO surface can also be used as a scaffold to immobilize various functional groups by weak interactions such as van der Waals forces, electrostatic interactions with negatively-charged surface oxygen functional groups, or π-π interactions with the delocalized π orbitals of the graphitic sp^2-carbon domains. In comparison with non-covalent functionalization, covalent synthetic strategies form more stable hybrid materials due to the strong bonds between the two components, and thereby facilitate effective electronic communication between the individual moieties in the hybrid. However, non-covalent functionalization can be beneficial in that it preserves the sp^2-conjugation of GO to a greater extent than covalent strategies such as diazotization, which causes local bond transformations from sp^2- to sp^3-hybridized sites. A wide range of functional species such as conjugated polymers, polyelectrolytes, nanoparticles, coordination complexes and organometallics, biomolecules such as DNA, proteins and enzymes surfactants, etc., have been attached via non-covalent strategies; more details can be found in reviews [126, 144, 146].

Although surface functionalization has great potential for combining the advantages of GO-based surfaces and appended functional moieties, it generally leads to a non-stoichiometric bulk functionalization across the carbon surface rather than a controlled uniform functionalization at each individual sheet; it is therefore extremely challenging to precisely manipulate the microstructure of the hybrid by selectively attaching a desired functional moiety at a precise location on the carbon backbone, or to control the number of functional moieties per individual GO/RGO sheet. The lack of appropriate analytical techniques with sufficient sensitivity is another drawback that has strongly hindered realizing the full

potential of GO-based hybrids. The "standard" characterization techniques such as liquid-state NMR spectroscopy, mass spectrometry, etc., which provide structural information at the molecular level, cannot be used in characterizing GO-based materials due to solubility issues; thus, multiple microscopic and spectroscopic characterization techniques that give complementary information are required to confirm the surface functionalization.

3.3.2. Third-order NLO and OL properties of GO-coordination complex hybrids

This section reviews the NLO and OL properties of coordination complex-functionalized GO-based hybrids assembled via various covalent functionalization strategies. Recent developments in GO-based hybrids of porphyrins, phthalocyanines and their metal-complexed derivatives are highlighted, due to their excellent optical nonlinearities that can be modulated through structural variations of both moieties. Further details on GO/RGO-based covalent and non-covalent hybrid materials and their NLO/OL properties can be found in several review papers [144, 145, 150-152].

Porphyrins and phthalocyanines are excellent NLO chromophores because of their highly delocalized extended π-conjugated macrocyclic structures. They possess large excited-state absorption cross-sections and long triplet excited-state life times, and they usually function as excellent RSA chromophores due to excited singlet- or excited triplet-state absorption (or both). Their architectural flexibility allows one to tune the NLO properties by manipulating the peripheral ring substituents, the central metal and its oxidation state, the

axial ligands attached to the central metal, the macrocycle composition, etc. [35, 41]. Both porphyrins and phthalocyanines show high linear transmission in the visible spectral range between their characteristic ground-state electronic absorption bands (i.e. between their B bands located at ca. 400 nm and their Q bands found at ca. 600 nm). This narrow transmission window can be extended by structural modifications at the macrocycle, so as to observe OL responses across a larger linear transmission window. Porphyrins and phthalocyanines are therefore excellent OL chromophores to graft to a GO-based platform in the design of efficient OL systems, by integrating their merit with the heterogeneous nonlinear dynamics of GO/RGO.

A wide range of metal-free and metalated porphyrins and phthalocyanines have been covalently anchored to GO-based platforms either via peripheral binding [18] or axial binding [153]. The covalent functionalization has generally been confirmed by a combination of characterization techniques, often including FTIR, XRD, TGA, and XPS, as well as Raman, UV-Vis absorption, steady-state and transient fluorescence spectroscopies, etc. The NLO and OL characteristics of these hybrids have been extensively studied using the Z-scan technique under different excitation conditions, the details of which are presented in Table 1. Most experimental studies have explored NLA-mediated OL but a few studies have reported Kerr nonlinearities [154, 155]. The level of detail of the NLO studies is variable; some studies have quantitatively investigated the NLO and OL performances of the hybrids by reporting NLA coefficients, absorption cross-sections, etc., while others are qualitative reports only. Discrepancies in data acquisition conditions and the imprecisely-defined nature of the hybrids render comparisons of NLO/OL data between

labs (and even between publications emanating from the same lab) fraught with difficulty. In the discussion that follows, we consider porphyrin hybrids followed by phthalocyanine hybrids and then metal alkynyl hybrids, and restrict the structure-property discussions to data from specific publications. Within the compound categories, free-base porphyrins are considered before metalated porphyrins, studies with GO before RGO, and syntheses employing amidation before those utilizing esterification and then other synthetic methods.

(Insert Table 1)

The first NLO and OL studies of a free-base porphyrin-functionalized GO nanohybrid were undertaken on **1** (Figure 8), which was prepared by covalently grafting an amino-functionalized 5,10,15,20-tetraphenylporphyrin to GO by an amidation reaction [18]. Steady-state fluorescence studies on **1** indicated efficient fluorescence quenching due to the strong photo-induced interactions between the 5,10,15,20-tetraphenylporphyrin unit and GO (electron and/or energy transfer from the photo-excited singlet porphyrin to the GO unit). The NLO and OL properties of **1** were assessed at 532 nm (ns time scale); enhanced NLO performance and OL properties were observed, in comparison to those of the individual (porphyrin and GO) components, their physical blend (1:1 weight ratio), and even better than the benchmark C_{60} at the same level of linear transmittance. The improved OL properties of the hybrid have been ascribed to a combination of RSA, 2PA, NLS, and photo-induced electron and/or energy transfer from the electron donor 5,10,15,20-tetraphenylporphyrin to the electron acceptor GO that leads to charge-separated excited states.

(Insert Figure 8)

Subsequently, 5,10,15,20-tetra(4-aminophenyl)porphyrin was linked to GO via amidation to afford **2** (Figure 9) [156]. The resultant hybrid exhibits enhanced NLO and OL properties at 532 nm in the ns pulse regime, in comparison to the performance of the individual components GO and porphyrin. The improved NLO performance of the hybrid was assigned to accumulation effects of 2PA, RSA, NLS and NLR from the hybrid components.

(Insert Figure 9)

Core-modified porphyrin-GO hybrids have been prepared by covalently linking mono(thia)porphyrin, di(thia)porphyrin, and tri(thia)sapphyrinon to GO via amidation to give **3**, **4**, and **5**, respectively (Figure 10) [157]. At identical linear transmittances, the nanohybrids exhibit enhanced NLO responses at 532 nm in the ns regime compared to the precursor GO and the modified porphyrins, a result ascribed to photo-induced electron or energy transfer from the singlet excited states of porphyrin to the GO and/or a combination of 2PA, RSA and/or NLS. The nonlinear responses follow the trend **3** > **5** > **4** > GO, with the magnitude dependent on the hyperpolarizability of the thiaporphyrins and the degree of electron or energy transfer from donor thiaporphyrin to the acceptor GO.

(Insert Figure 10)

In addition to free-base porphyrins, there have been several reports of the NLO and OL properties of GO covalently anchored to metalated porphyrins. The reason for the interest in metalated porphyrins is that they exhibit better optical nonlinearities than free-base

porphyrins due to the enhanced efficiency of the ISC process which results from spin-orbit coupling; tuning the central metal atom in the macrocycle can therefore be an effective design strategy to modulate the NLO properties of porphyrin-GO-based hybrids [158].

Enhanced NLO and OL properties at 532 nm in the ns regime were observed for graphene hybrids of porphyrins metalated with copper and zinc in comparison to the performance of their individual components [159]. The 2PA coefficient of the Cu porphyrin-graphene hybrid was found to be about thirty-five times larger than copper porphyrin, while the coefficient for the Zn porphyrin-graphene hybrid was about ten times larger than that of the zinc porphyrin. The improved NLO and OL performance was assigned to 2PA, ESA, NLS and energy transfer from porphyrin to graphene due to the covalent linkage between GO and the porphyrin. Energy transfer from the excited states of porphyrins to the GO enhances the 2PA of porphyrins and allows fast non-radiative relaxation from the excited states of GO to the ground state, contributing to the OL.

Free-base and metal-complexed 5-(4-aminophenyl)-10,15,20-tri(4-tolyl)porphyrins of Zn, Cu, Sn and VO were covalently attached to GO by esterification to afford **6** (Figure 11) [160]. Fluorescence quenching was observed in the hybrids, a common motif for this material type, and was ascribed to strong electronic interactions between the porphyrin and GO components. The NLO and OL properties of **6** were then assessed at 532 nm with ns pulses and at 800 nm with fs laser pulses. With ns laser pulse excitation, the nanohybrids **6** showed 2PA and ESA-dominant NLA behaviour leading to RSA, while in the fs pulse regime, SA was dominant. With ns laser pulses, the 2PA coefficients of all porphyrin-GO hybrids were found to be significantly larger than those of GO and porphyrins due to strong

2PA, ESA and nonlinear scattering. In comparison to the metalated GO hybrids (**6**, M = Sn, VO) and GO, the free-base porphyrin-GO hybrid exhibited enhanced NLA and the highest 2PA coefficient in the ns regime.

(Insert Figure 11)

Covalently linked GO-porphyrin hybrids (both the free base and Cu, Zn, and Sn metalated) were prepared via esterification and their NLO properties explored, in further studies examining the effect of varying the central metal atom and pulse width on the NLO and OL performance [161]. The NLO and OL properties were examined at 532 nm in the ps regime and 800 nm in the fs regime. The hybrids exhibited higher damage thresholds in both pulse regimes. The free-base porphyrins transform from RSA to SA in behaviour in the ps regime upon increasing the laser intensity, due to singlet excited-state saturation by 2PA at higher intensities, but in contrast, the hybrids showed the reverse behaviour in the ps regime, switching from RSA to SA and then returning to RSA with increasing intensity, due to the strong 2PA contribution from the GO component. The absorption spectra have been analysed to shed light on these interesting observations; energy transfer from the porphyrin excited states to the GO bands has been suggested to enhance the 2PA of the porphyrins, while GO inhibits the SA behaviour by means of ultrafast relaxation of the excited states to the ground states. This intensity-dependent switching of RSA to SA and back to RSA is of applications interest, with potential use in ultrafast nonlinear optical switching. In the fs regime, SA behaviour is dominant, in agreement with the aforementioned studies. No scattering signals were observed for GO or the hybrids due to the comparatively low fluencies employed for both the ps and fs pulses.

The effect of axial coordination at the metal porphyrin component of the (R)GO-porphyrin hybrids on the NLO properties has also been examined [153, 162]. Two axially-coordinated porphyrins, a tin(IV)-cored porphyrin (**7**) and a phosphorus-cored porphyrin (**8**) (Figure 12), have been synthesized by esterification at the Sn-OH and deprotonation of GO hydroxyl followed by nucleophilic substitution at P-Cl [153]. At identical concentrations, **7** and **8** exhibit enhanced NLO performance and broadband OL properties at 532 nm in both the ns and ps regimes compared to the precursor porphyrins and GO. A combination of NLS and/or 2PA, RSA and photo-induced electron transfer or energy transfer from the electron-donor porphyrin moieties to the -acceptor GO have been suggested to be responsible for the improved optical nonlinearities of the hybrids.

(Insert Figure 12)

RGO was functionalized with mono-substituted 5,10,15,20-tetraphenylporphyrins by two distinct procedures involving 1,3-dipolar cycloadditions to give **9** and **10**, which differ in the degree of porphyrin functionalization of RGO (Figure 13) [154]. At the same linear transmittance in the ns regime at 532 nm, both RGO-porphyrin conjugates **9** and **10** show increased NLO and OL responses in comparison to the precursor RGO and the free-base porphyrins. Multiple nonlinear effects (RSA, NLS, and photo-induced electron transfer from the electron-donor 5,10,15,20-tetraphenylporphyrin unit to the electron-acceptor RGO) contribute to the improvement in optical nonlinearities on progressing to the hybrids, while interband transitions of defect-induced states through ESA may be responsible for the enhanced OL responses of the hybrids. Closed-aperture Z-scan studies of RGO exhibited positive nonlinear refraction (or self-focusing) and of the porphyrins exhibited

negative nonlinear refraction (self-defocusing), while both **9** and **10** exhibited positive nonlinear refraction effects, indicating RGO dominates the nonlinear refractive behaviour of the hybrids.

(Insert Figure 13)

Coupling of free-base porphyrins to RGO by means of diazonium species has also been explored [163]. Diazotization of 5-(4-aminophenyl)-10,15,20-triphenylporphyrin and reaction of the resultant diazonium with RGO gave **11**, while in an alternative stepwise synthesis, 4-aminophenol was diazotized and attached to RGO to afford RGO with a pendant -OH functionality, and then a tetraphenylporphyrin derivative was added to RGO via a nucleophilic substitution reaction to afford **12** (Figure 14). UV-Vis absorption spectroscopy and steady-state fluorescence studies suggest π-π interactions and photo-induced electron and/or energy transfer between the porphyrin units and the RGO surface. The NLO properties of the hybrids and their precursors have been assessed with both ns and ps laser pulses at 532 nm. In the ps regime, RGO exhibits SA behaviour while RSA dominates in the ns regime, whereas the free porphyrins display RSA-dominated nonlinear absorption in both the ps and ns regimes. The RGO-TPP hybrids exhibit improved NLA responses in comparison to the individual components and the benchmark C_{60} in both pulse regimes, with superior NLA responses being observed with the longer ns laser pulses than the shorter ps pulses. The improved NLO properties of the hybrids have been ascribed to a combination of NLO effects originating from the RGO and porphyrin moieties as well as electron and/or energy transfer interactions via the covalent linkage, an outcome consistent with the aforementioned studies.

(Insert Figure 14)

Sn-metalated porphyrins have been attached to RGO and the NLO properties of the resultant hybrids assessed [162]. Phenol groups were first anchored to the RGO surface via 1,3-dipolar cycloaddition or diazotization, and then tetraphenylporphyrins metalated with dichlorotin units were covalently attached by nucleophilic substitution to afford **13** and **14** (Figure 15). The RGO-porphyrin nanohybrids exhibit larger NLO responses at 532 nm in both the ns and ps regimes than the precursors, due to the combination of NLO mechanisms reported above for similar hybrid systems. The hybrids show SA-dominated NLA in the ps regime and RSA-dominated NLA in the ns regime, with the NLA responses increasing in the order RGO < **13** < **14**, the covalent linkage between the two moieties and the difference in the synthetic routes used to prepared the hybrids influencing the efficiency.

(Insert Figure 15)

Metalated porphyrins have also been attached to GO and RGO by means of poly(arylene ether sulfone), which was anchored to the surface through an amide linkage (Figure 16) [164]. This design strategy not only enhances the optical nonlinearities but also improves the solubility and processability in different organic solvents. The resultant porphyrinated polymer-functionalized GO hybrid, **15**, was reduced to **15-RGO** by hydrazine, restoring the sp^2 conjugation of the GO backbone. A polymer-free zinc-functionalized tri(naphthyl)porphyrin GO hybrid was synthesized as a reference hybrid by esterification, and then also reduced by hydrazine. The NLO and OL performances of these hybrids and their precursors have been examined at 532 nm and 1064 nm on the ns time scale. At

equivalent linear transmittance, the porphyrinated-polymer GO/RGO hybrids **15** and **15-RGO** exhibit superior NLO performance to the individual components as well as the polymer-free hybrids. **15** and **15-RGO** possess the largest effective nonlinear absorption coefficients (β_{eff}) at both 532 and 1034 nm, which has been suggested to stem from a combination of RSA, NLS, and photo-induced electron and/or energy transfer via the polyaryl-polymer backbones. The β_{eff} values of **15** and **15-RGO** are five times and seven times larger than the precursor GO at 532 nm, respectively, while **15-RGO** exhibits a β_{eff} value thirty times larger than that of GO at 1034 nm. In comparison to the zinc-functionalized tri(naphthyl)porphyrin GO hybrid and **15**, the corresponding RGO hybrids show stronger NLO responses and OL effects due to ESA-dominated NLA originating from restoration of the sp^2 conjugation.

(Insert Figure 16)

Phthalocyanine is, similar to porphyrin, a promising π-conjugated chromophore with large third-order nonlinearities that has huge potential in combination with GO/RGO. A number of studies have reported the influence of the phthalocyanine moiety on the NLO and OL performance of GO-based hybrids, exploring the effects of varying the central metal atom, the electron-donating peripheral substituents, the position of the substituents, etc., and have shown remarkable accumulation effects via the covalent linkage between the GO/RGO and phthalocyanine units; the details of these studies are collected in Table 2.

(Insert Table 2)

For example, an unsymmetrically-substituted zinc phthalocyanine has been covalently linked to GO by amidation and the NLO and OL performance of the resulting hybrid **16** (Figure 17) has been studied at 532 nm and 1064 nm employing ns pulses [165]. Steady-state fluorescence spectra indicate fluorescence quenching in the GO-PcZn hybrid due to electron-transfer from the electron-donor zinc phthalocyanine unit to the electron-acceptor GO moiety. GO exhibits 2PA/NLS-dominated OL responses at 532 nm and NLS-dominated OL at 1064 nm, whereas the free unsymmetrically-substituted zinc phthalocyanine shows an RSA-dominated OL response at 532 nm without any significant nonlinear effects at 1034 nm. At the same concentration, **16** displays stronger NLO effects and a better OL performance than GO or the free unsymmetrically-substituted zinc phthalocyanine at 532 nm due to multiple NLO mechanisms arising from the individual moieties (RSA from the zinc phthalocyanine and 2PA/NLS from GO). Surprisingly, **16** exhibits a greater OL response at 1064 nm than the precursor GO although the zinc phthalocyanine is OL-inactive at 1064 nm; the reason for this is unclear.

(Insert Figure 17)

The effect of varying the degree of oxidation of GO on the optical nonlinearities of phthalocyanine-GO hybrids has been assessed [166]. Three different graphitic surfaces, namely pure graphene (G), graphene oxide (GO), and reduced graphene oxide (RGO), have been covalently functionalized with zinc 2,9,16,23-tetra(amino)phthalocyanine via amidation and the NLO and OL properties of the resulting hybrids G-ZnPc, GO-ZnPc and RGO-ZnPc have been studied at 532 nm in the ns and fs regimes at the same concentration. In the ns regime, RGO-ZnPc shows a better NLO and OL performance with a larger

nonlinear absorption coefficient than the other hybrids, individual RGO, zinc 2,9,16,23-tetra(amino)phthalocyanine, or a physical blend of RGO and zinc 2,9,16,23-tetra(amino)phthalocyanine, and indeed even larger than that of the benchmark material C_{60}. In the fs regime, GO-ZnPc shows the best NLO performance of the hybrids. The enhanced NLO properties have been suggested to originate from a combination of NLS, RSA, and efficient light-induced energy or electron transfer from the electron-donor ZnPc unit to the electron-acceptor RGO moiety.

Axially-substituted phthalocyanines are interesting due to the dipole moment oriented perpendicular to the macrocycle plane. The gallium phthalocyanine-GO hybrid **17** (Figure 18) has been synthesized by reacting the Ga-Cl functionality of the tetrakis(*tert*-butyl)phthalocyanine gallium chloride precursor with the hydroxyl groups on the basal planes of GO in the presence of carbonate as base [167]. The NLO properties of the hybrid **17**, the precursors, and benchmark C_{60} have been studied at the same concentration using ns laser pulses at 532 nm and 1064 nm. **17** has the largest NLA coefficient and OL performance due to NLS, RSA, and 2PA and accumulation effects from the covalent linkage between the GO and phthalocyanine moieties. Interestingly, **17** exhibits a better OL response than GO at 1064 nm, although the phthalocyanine is OL-inactive and **17** shows a weaker scattering response than GO at 1064 nm; the reason for the greater OL ability of **17** at 1064 nm is unclear.

(Insert Figure 18)

The RGO-zinc phthalocyanine hybrid **18** has been prepared by an esterification reaction between zinc tetrakis(2-[2-(2-hydroxyethoxy)ethoxy]ethoxy)phthalocyanine and GO (which affords the GO-zinc phthalocyanine hybrid GO-ZnPc), and a subsequent in situ reduction to **18** following mild thermal treatment in DMF (Figure 19) [168]. NLO and OL studies have been carried out with 532 nm, ns laser excitation, showing that the GO-ZnPc hybrid possesses better nonlinear responses than the precursor components, a result consistent with cumulative NLA effects originating from the GO and the zinc phthalocyanine moieties via the covalent linkage. The in situ reduced hybrid **18** shows a further enhancement in the NLA responses and efficiency in OL (and possesses the highest nonlinear absorption coefficient), presumably due to the restoration of the π-conjugated network following thermal reduction.

(Insert Figure 19)

The effect of varying the central metal atom in the phthalocyanine on the NLO and OL properties of the GO-based hybrids has also been assessed. Metal(II) phthalocyanines have been linked to RGO (following the same synthetic approach that was previously used in synthesizing **19** to give **20** (M = Cu, Pb) (Figure 20) [155]. The NLO and OL properties of the resulting metal phthalocyanine hybrids **19** and **20** and the precursor phthalocyanines have been studied using the open- and closed-aperture Z-scan techniques at 532 nm in the ns laser pulse regime. All metal phthalocyanines display RSA-dominated NLA, with nonlinear absorption coefficients that increase in the order Zn < Pb < Cu. However, the hybrids **19** and **20** show the inverse order in nonlinear absorption coefficients, namely Zn > Pb > Cu. This change in the NLO responses in the hybrids has been suggested to arise

from photo-induced electron transfer or energy-transfer between the RGO and the MPc moieties, rather than a contribution from the MPc moieties in the hybrid. The closed-aperture Z-scan measurements of the hybrids revealed self-focusing behaviour while the MPc molecules did not show nonlinear refractive effects.

(Insert Figure 20)

The influence of peripheral substitution at phthalocyanines on the NLO properties of their GO-based hybrids has also been studied [169]. 1,8,15,22-tetra(3-(5-hydroxyl)pentyloxy)phthalocyanine zinc ($ZnPc(TD)_4$) and 1,8,15,22-tetra-(3-[2-(2-hydroxyl)ethoxy]ethoxy)phthalocyanine zinc ($ZnPc(DG)_4$) have been attached to GO by means of esterification reactions, affording the corresponding hybrids **21** and **22**. NLO studies at 532 nm in the ns regime have revealed that $ZnPc(DG)_4$ has a larger NLA coefficient than $ZnPc(TD)_4$, a result which is suggested to stem from the increased electron density in the former facilitating more efficient ISC and thereby improving the third-order nonlinearity. The hybrids display the same trend, **22** having a larger NLA coefficient than **21**. The improved NLO performance of the hybrids has been assigned to a combination of the NLA mechanisms of the GO and phthalocyanine zinc moieties, including 2PA originating from the sp^3 carbons in the GO, ESA from the small localized sp^2 regions in the GO, SA from sp^2 carbon clusters in the GO, ESA from the ZnPc units, and photo-induced electron and/or energy transfer between the GO and ZnPc moieties in the hybrids.

(Insert Figure 21)

Amidation as a means to functionalize GO with phthalocyanines has also been exploited by functionalization of the GO surface with amines followed by reaction of the aminated GO with carboxylic acid-functionalized phthalocyanines. Specifically, ethylenediamine has been added to GO nanosheets to give a GO-ethylenediamine adduct, and the pendant amino groups of the adduct have then been reacted with the carboxyl functional groups of a tetracarboxylic acid-functionalized phthalocyanine zinc(II) to afford the amide-containing hybrids [170]. Hybrids have also been synthesized by esterification. The NLO properties have been explored with 532 nm ns laser pulses, the enhanced NLA in the amide-containing hybrids being suggested to arise from the combined effects of ESA derived from the extended sp^2-carbon configurations of the amide-containing moiety, RSA derived from the phthalocyanine units, and efficient photo-induced electron and/or energy transfer from the electron-donor phthalocyanines to the amide-containing GO sheets. Both hybrids exhibit larger nonlinear absorption coefficients than their precursors, but the amide-containing hybrids have a higher value of the coefficient due to the ethylenediamine partially restoring the conjugation of GO.

The effect of introducing amino groups at the two distinct arene sites of phthalocyanines on the NLO properties of their hybrids with GO has also been explored. The two tetra(amino)phthalocyanine zinc isomers have been attached to GO via amidation, to afford the hybrids **23** and **24** (Figure 22) [171]. The NLO properties of the hybrids have been studied at 532 nm on the ns time scale; they show larger values of the NLA coefficient than GO or the free phthalocyanines, the larger NLA effects being suggested to derive from a combination of the NLO effects originating from the GO and phthalocyanine moieties as

well as photo-induced electron and/or energy transfer between the components. Intramolecular hydrogen bonding in **23** reduces its electron-donating ability and thus the photo-induced electron transfer/energy transfer and, as a result, **24** exhibits stronger NLA than **23**.

(Insert Figure 22)

As discussed above, metalated porphyrins and phthalocyanines are the major types of coordination complex that have been covalently linked to GO/RGO surfaces with the intent of modulating the NLO and OL properties. Transition metal σ-alkynyl complexes are another interesting class of NLO/OL chromophore, due to the large nonlinear effects and the architectural flexibility that facilitates optimization of the NLO properties over a broad range [8, 172, 173]. However, metal σ-alkynyl complex/GO hybrids have not thus far been explored extensively for NLO and OL applications. Cyclometalated square-planar Pt(II) complexes have been attached covalently to GO via amidation to afford **25** and by means of electrostatic adsorption to give **26** (Figure 23; the experimental details are collected in Table 3) [174]. The NLO and OL properties of these hybrids and their precursors have been investigated by open-aperture Z-scan (532 nm ns pulses). In agreement with observations for the porphyrin- and phthalocyanine-based GO/RGO hybrids, the hybrids **25** and **26** exhibit much greater NLO and OL performance compared to the performance of the individual components, an outcome suggested to arise from the synergistic effects of NLS and TPA of the GO, RSA from the Pt complexes, and photo-induced electron and energy transfer from the Pt complexes to GO. The NLO and OL data for **26** are larger than those of **25** due to the better OL performance of the platinum-containing precursor of the former,

the bonding between the two moieties, and the higher degree of GO functionalization for **26**.

(Insert Figure 23)

(Insert Table 3)

The studies thus far suggest that covalent functionalization is an effective design strategy to simultaneously combine or modulate the heterogeneous NLO dynamics of the GO/RGO surfaces with the complementary nonlinear mechanisms of potential coordination complex chromophores, but considerable research still needs to be done to optimize the NLO responses of the hybrids via (i) tuning the degree of functionalization (or the number of functional moieties per area of GO/RGO), (ii) incorporating other potential coordination complex chromophores and (iii) exploring different design strategies.

4. Summary and outlook

Materials able to manipulate the intensity or the fluence of photonic signals have enormous importance in optoelectronic applications, in particular for sensor protection against intense laser radiation. In recent years, there has been a growing research interest in the rational design and fabrication of NLO media with sufficiently large nonlinear responses suitable for practical OL devices. GO and RGO are interesting NLO media owing to their large third-order optical nonlinearities and efficient OL responses which can be tuned by modifying the sp^2- and sp^3-carbon content. Their tunable carbon platforms can be

effectively integrated with a wide range of complementary NLO moieties via different covalent and non-covalent surface functionalization strategies to build up multifunctional hybrid architectures. Among the diverse range of coordination complex-based GO/RGO hybrid systems, porphyrins and phthalocyanines are the most extensively explored. Their GO/RGO hybrids have shown improved NLO and OL performance in comparison with the individual functional components due to multiple NLA effects such as 2PA, RSA and ESA, NLS and photo-induced electron and/or energy transfer between GO/RGO and the macrocyclic moiety through the covalent linkage. These covalent conjugates merge the OL merits of the π-conjugated organic macrocycles with the heterogeneous nonlinear dynamics of GO/RGO.

However, a significant amount of research still needs to be done to unravel the OL potential of the coordination complex moieties covalently attached to GO/RGO and to further optimize the OL efficiency of the hybrid systems. This can be achieved by harnessing the OL merit of both the coordination complex and the GO/RGO platform at their fullest potential via suitable hybridization strategies. Systematic studies are required to explore the modifications in the NLO and OL responses of the hybrid as a function of the degree of functionalization per unit area of the GO/RGO sheet of a particular hybrid structure. It is also necessary to systematically study the effect of employing different covalent binding strategies of a coordination complex to a carbon platform on the optical nonlinearities of the resultant hybrids. Another potential avenue to tune the optical nonlinearities of the hybrids is the design of novel hybrid materials incorporating other organometallic and/or coordination complexes with large nonlinearities such as transition metal alkynyl

complexes, and extending from classical dipolar donor-bridge-acceptor examples to branched systems with multipolar charge distributions. Replacement of the carbon platform of GO/RGO with other sp^2 conjugated nanocarbon platforms such as carbon nanotubes, fullerenes, graphene, etc., and a systematic study of the effect of these modifications on the NLO and OL properties are needed. Hybrids should also be introduced into host solid matrices such as polymers, and thereby made available in the form of thin films, to explore their potential in fabricating practical OL devices. Finally, it is important to expand the understanding of the interfacial binding and the distribution of the coordination complexes on the carbon surface; this is an extremely difficult challenge due to the lack of instrumentation affording conclusive structural information and the highly heterogeneous nature of these materials.

5. Acknowledgement

We thank the Australian Research Council (ARC) for financial support. D.M.A.S.D. was the recipient of an Australian Postgraduate Award.

6. References

[1] L.W. Tutt, T.F. Boggess, Prog. Quantum Electron. 17 (1993) 299.

[2] D. Dini, M.J.F. Calvete, M. Hanack, Chem. Rev. 116 (2016) 13043.

[3] P.J. Smalley, Laser Therapy 20 (2011) 95.

[4] D.J. Harter, M.L. Shand, Y.B. Band, J. Appl. Phys. 56 (1984) 865.

[5] Y.B. Band, D.J. Harter, R. Bavli, Chem. Phys. Lett. 126 (1986) 280.

[6] G.S. He, Nonlinear Optics and Photonics, Oxford University Press, Oxford, UK, 2015.

[7] J. Wang, J.B. Werner, J. Opt. A: Pure Appl. Opt. 11 (2009) 024001.

[8] G.J. Zhou, W.Y. Wong, Chem. Soc. Rev. 40 (2011) 2541.

[9] Y.P. Sun, J.E. Riggs, Int. Rev. Phys. Chem. 18 (1999) 43.

[10] Y. Zhang, Y. Wang, RSC Adv. 7 (2017) 45129.

[11] K. Sridharan, M.S. Ollakkan, R. Philip, T.J. Park, Carbon 63 (2013) 263.

[12] J. Wang, D. Früchtl, Z. Sun, J.N. Coleman, W.J. Blau, J. Phys. Chem. C 114 (2010) 6148.

[13] F.E. Hernández, W. Shensky, I. Cohanoschi, D.J. Hagan, E.W. van Stryland, Appl. Opt. 41 (2002) 1103.

[14] L. François, M. Mostafavi, J. Belloni, J.F. Delouis, J. Delaire, P. Feneyrou, J. Phys. Chem. B 104 (2000) 6133.

[15] R. West, Y. Wang, T. Goodson, J. Phys. Chem. B 107 (2003) 3419.

[16] J. Wang, W.J. Blau, J. Phys. Chem. C 112 (2008) 2298.

[17] S.R. Mishra, H.S. Rawat, M.P. Joshi, S.C. Mehendale, J. Phys. B 27 (1994) L157.

[18] Y. Xu, Z. Liu, X. Zhang, Y. Wang, J. Tian, Y. Huang, Y. Ma, X. Zhang, Y. Chen, Adv. Mater. 21 (2009) 1275.

[19] O. Durand, V. Grolier-Mazza, R. Frey, J. Opt. Soc. Am. B. 16 (1999) 1431.

[20] D. Vincent, S. Petit, S.L. Chin, Appl. Opt. 41 (2002) 2944.

[21] K. Mansour, M.J. Soileau, E.W. van Stryland, J. Opt. Soc. Am. B 9 (1992) 1100.

[22] N.M.B. Neto, C.R. Mendonça, L. Misoguti, S.C. Zilio, Appl. Phys. B 78 (2004) 1.

[23] K.J. McEwan, P.A. Madden, J. Chem. Phys. 97 (1992) 8748.

[24] T. Xia, A. Dogariu, K. Mansour, D.J. Hagan, A.A. Said, E.W. van Stryland, S. Shi, J. Opt. Soc. Am. B. 15 (1998) 1497.

[25] S.M. King, S. Chaure, J. Doyle, A. Colli, A.C. Ferrari, W.J. Blau, Opt. Commun. 276 (2007) 305.

[26] R.A. Ganeev, A.I. Ryasnyansky, S.R. Kamalov, M.K. Kodirov, T. Usmanov, J. Phys. D 34 (2001) 1602.

[27] V. Joudrier, P. Bourdon, F. Hache, C. Flytzanis, Appl. Phys. B 70 (2000) 105.

[28] M. Sheik-Bahae, A.A. Said, E.W. van Stryland, Opt. Lett. 14 (1989) 955.

[29] M. Sheik-Bahae, D.J. Hagan, E.W. van Stryland, Phys. Rev. Lett. 65 (1990) 96.

[30] S.M. Shivashankar, V.K. Anantapadmanabha, A.V. Adhikari, Polym. Eng. Sci. 53 (2013) 1347.

[31] H. Wang, Z. Li, B. Huang, Z. Jiang, Y. Liang, H. Wang, J. Qin, G. Yu, Y. Liu, Y. Song, React. Funct. Polym. 66 (2006) 993.

[32] C. Li, C. Liu, Q. Li, Q. Gong, Chem. Phys. Lett. 400 (2004) 569.

[33] G.S. He, J.D. Bhawalkar, C.F. Zhao, P.N. Prasad, Appl. Phys. Lett. 67 (1995) 2433.

[34] J.E. Riggs, R.B. Martin, D.B. Walker, Z. Guo, Y.-P. Sun, Phys. Chem. Chem. Phys. 6 (2004) 703.

[35] M.O. Senge, M. Fazekas, E.G.A. Notaras, W.J. Blau, M. Zawadzka., O.B. Locos, E.M.N. Mhuircheartaigh, Adv. Mater. 19 (2007) 2737.

[36] W. Blau, H. Byrne, W.M. Dennis, J.M. Kelly, Opt. Commun. 56 (1985) 25.

[37] F.Z. Henari, W.J. Blau, L.R. Milgrom, G. Yahioglu, D. Phillips, J.A. Lacey, Chem. Phys. Lett. 267 (1997) 229.

[38] J.J. Doyle, J. Wang, S.M. O'Flaherty, Y. Chen, A. Slodek, T. Hegarty, I.L.E. Carpenter, D. Wöhrle, M. Hanack, W.J. Blau, J. Opt. A: Pure Appl. Opt. 10 (2008) 075101.

[39] S.M. O'Flaherty, S.V. Hold, M.J. Cook, T. Torres, Y. Chen, M. Hanack, W.J. Blau, Adv. Mater. 15 (2003) 19.

[40] Y. Chen, M. Hanack, Y. Araki, O. Ito, Chem. Soc. Rev. 34 (2005) 517.

[41] G.de la Torre, P. Vázquez, F. Agulló-López, T. Torres, J. Mater. Chem. 8 (1998) 1671.

[42] G. de la Torre, P. Vázquez, F. Agulló-López, T. Torres, Chem. Rev. 104 (2004) 3723.

[43] C. Zhang, Y. Song, X. Wang, Coord. Chem. Rev. 251 (2007) 111.

[44] R. Philip, G.R. Kumar, N. Sandhyarani, T. Pradeep, Phys. Rev. B 62 (2000) 13160.

[45] S. Qu, C. Du, Y. Song, Y. Wang, Y. Gao, S. Liu, Y. Li, D. Zhu, Chem. Phys. Lett. 356 (2002) 403.

[46] S. Porel, S. Singh, S.S. Harsha, D.N. Rao, T.P. Radhakrishnan, Chem. Mater. 17 (2005) 9.

[47] W. Sun, Q. Dai, J.G. Worden, Q. Huo, J. Phys. Chem. B 109 (2005) 20854.

[48] H.I. Elim, J. Yang, J.Y. Lee, J. Mi, W. Ji, Appl. Phys. Lett. 88 (2006) 083107.

[49] S.L. Smitha, K.G. Gopchandran, N. Smijesh, R. Philip, Prog. Nat. Sci. 23 (2013) 36.

[50] H. Pan, W. Chen, Y.P. Feng, W. Ji, J. Lin, Appl. Phys. Lett. 88 (2006) 223106.

[51] W. Jia, E.P. Douglas, F. Guo, W. Sun, Appl. Phys. Lett. 85 (2004) 6326.

[52] E.W. van Stryland, Y.Y. Wu, D.J. Hagan, M.J. Soileau, K. Mansour, J. Opt. Soc. Am. B. 5 (1988) 1980.

[53] A.A. Said, M. Sheik-Bahae, D.J. Hagan, T.H. Wei, J. Wang, J. Young, E.W. van Stryland, J. Opt. Soc. Am. B 9 (1992) 405.

[54] Q. Chang, C. Chang, X. Zhang, H. Ye, G. Shi, W. Zhang, Y. Wang, X. Xin, Y. Song, Opt. Commun. 274 (2007) 201.

[55] G.S. He, K.T. Yong, Q. Zheng, Y. Sahoo, A. Baev, A.I. Ryasnyanskiy, P.N. Prasad, Opt. Express 15 (2007) 12818.

[56] C.E. Powell, M.G. Humphrey, Coord. Chem. Rev. 248 (2004) 725.

[57] R. Vestberg, R. Westlund, A. Eriksson, C. Lopes, M. Carlsson, B. Eliasson, E. Glimsdal, M. Lindgren, E. Malmström, Macromolecules 39 (2006) 2238.

[58] A. Baev, O. Rubio-Pons, F. Gel'mukhano, H. Ågren, J. Phys. Chem. A 108 (2004) 7406.

[59] F. Guo, W. Sun, Y. Liu, K. Schanze, Inorg. Chem. 44 (2005) 4055.

[60] K.B. Manjunatha, R. Ravindra, G. Umesh, B.R. Bhat, P. Poornesh, Laser Phys. 27 (2017) 085401.

[61] H.C. Sampath Kumar, B. Ramachandra Bhat, B.J. Rudresha, R. Ravindra, R. Philip, Chem. Phys. Lett. 494 (2010) 95.

[62] L.Y. Kong, Z.W. Li, T. Okamura, G.H. Ma, Q. Chu, H.F. Zhu, S.H. Tang, W.Y. Sun, N. Ueyama, Chem. Phys. Lett. 416 (2005) 176.

[63] Y.P. Sun, J.E. Riggs, B. Liu, Chem. Mater. 9 (1997) 1268.

[64] S.S. Harilal, C.V. Bindhu, V.P.N. Nampoori, C.P.G. Vallabhan, J. Appl. Phys. 86 (1999) 1388.

[65] M.P. Joshi, S.R. Mishra, H.S. Rawat, S.C. Mehendale, K.C. Rustagi, Appl. Phys. Lett. 62 (1993) 1763.

[66] D.G. McLean, R.L. Sutherland, M.C. Brant, D.M. Brandelik, P.A. Fleitz, T. Pottenger, Opt. Lett. 11 (1993) 858.

[67] F. Henari, J. Callaghan, H. Stiel, W. Blau, D.J. Cardin, Chem. Phys. Lett. 199 (1992) 144.

[68] G. Brusatin, R. Signorini, J. Mater. Chem. 12 (2002) 1964.

[69] L.W. Tutt, A. Kost, Nature 356 (1992) 225.

[70] D. Vincent, J. Cruickshank, Appl. Opt. 36 (1997) 7794.

[71] J. Wang, W.J. Blau, Appl. Phys. B 91 (2008) 521.

[72] S.R. Mishra, H.S. Rawat, S.C. Mehendale, K.C. Rustagi, A.K. Sood, R. Bandyopadhyay, A. Govindaraj, C.N.R. Rao, Chem. Phys. Lett. 317 (2000) 510.

[73] N. Kamaraju, S. Kumar, A.K. Sood, S. Guha, S. Krishnamurthy, C.N.R. Rao, Appl. Phys. Lett. 91 (2007) 251103.

[74] L. Vivien, P. Lançon, D. Riehl, F. Hache, E. Anglaret, Carbon 40 (2002) 1789.

[75] J. Wang, Y. Chen, W.J. Blau, J. Mater. Chem. 19 (2009) 7425.

[76] J.E. Riggs, D.B. Walker, D.L. Carroll, Y.P. Sun, J. Phys. Chem. B 104 (2000) 7071.

[77] Z. Sun, T. Hasan, F. Torrisi, D. Popa, G. Privitera, F. Wang, F. Bonaccorso, D.M. Basko, A.C. Ferrari, ACS Nano 4 (2010) 803.

[78] M. Feng, H. Zhan, Y. Chen, Appl. Phys. Lett. 96 (2010) 033107.

[79] J. Wang, Y. Hernandez, M. Lotya, J.N. Coleman, W.J. Blau, Adv. Mater. 21 (2009) 2430.

[80] Q. Bao, H. Zhang, Y. Wang, Z. Ni, Y. Yan, Z.X. Shen, K.P. Loh, D.Y. Tang, Adv. Funct. Mater. 19 (2009) 3077.

[81] N. Liaros, P. Aloukos, A. Kolokithas-Ntoukas, A. Bakandritsos, T. Szabo, R. Zboril, S. Couris, J. Phys. Chem. C 117 (2013) 6842.

[82] Z.B. Liu, X. Zhao, X.L. Zhang, X.Q. Yan, Y.P. Wu, Y.S. Chen, J.G. Tian, J. Phys. Chem. Lett. 2 (2011) 1972.

[83] X.F. Jiang, L. Polavarapu, S.T. Neo, T. Venkatesan, Q.H. Xu, J. Phys. Chem. Lett. 3 (2012) 785.

[84] X. Zheng, M. Feng, H. Zhan, J. Mater. Chem. C 1 (2013) 6759.

[85] H. Shi, C. Wang, Z. Sun, Y. Zhou, K. Jin, S.A.T. Redfern, G. Yang, Opt. Express 22 (2014) 19375.

[86] N. Liaros, E. Koudoumas, S. Couris, Appl. Phys. Lett. 104 (2014) 191112.

[87] N. Liaros, J. Tucek, K. Dimos, A. Bakandritsos, K.S. Andrikopoulos, D. Gournis, R. Zboril, S. Couris, Nanoscale 8 (2016) 2908.

[88] X. Zheng, B. Jia, X. Chen, M. Gu, Adv. Mater. 26 (2014) 2699.

[89] Y. Gan, M. Feng, H. Zhan, Appl. Phys. Lett. 104 (2014) 171105.

[90] K.C. Chin, A. Gohel, W.Z. Chen, H.I. Elim, W. Jia, G.L. Chong, C.H. Sow, A.T.S. Wee, Chem. Phys. Lett. 409 (2005) 85.

[91] N. Izard, C. Ménard, D. Riehl, E. Doris, C. Mioskowski, E. Anglaret, Chem. Phys. Lett. 391 (2004) 124.

[92] S. Webster, M. Reyes-Reyes, X. Pedron, R. López-Sandoval, M.M. Terrones, D.L. Carroll, Adv. Mater. 17 (2005) 1239.

[93] É.M.N. Mhuircheartaigh, S. Giordani, W.J. Blau, J. Phys. Chem. B 110 (2006) 23136.

[94] L. Peipei, N. Lijuan, C. Yu, W. Jun, L. Ying, Z. Jinjuan, J.B. Werner, Nanotechnology 22 (2011) 015204.

[95] Z.B. Liu, J.G. Tian, Z. Guo, D.M. Ren, F. Du, J.Y. Zheng, Y.S. Chen, Adv. Mater. 20 (2008) 511.

[96] N. He, Y. Chen, J. Bai, J. Wang, W.J. Blau, J. Zhu, J. Phys. Chem. C 113 (2009) 13029.

[97] K.S. Liao, J. Wang, D. Früchtl, N.J. Alley, E. Andreoli, E.P. Dillon, A.R. Barron, H. Kim, H.J. Byrne, W.J. Blau, S.A. Curran, Chem. Phys. Lett. 489 (2010) 207.

[98] S.M. O'Flaherty, R. Murphy, S.V. Hold, M. Cadek, J.M. Coleman, W.J. Blau, J. Phys. Chem. B 107 (2003) 958.

[99] N. Sun, Y. Wang, Y. Song, Z. Guo, L. Dai, D. Zhu, Chem. Phys. Lett. 344 (2001) 277.

[100] Z.B. Liu, Y.F. Xu, X.Y. Zhang, X.L. Zhang, Y.S. Chen, J.G. Tian, J. Phys. Chem. B 113 (2009) 9681.

[101] P. Zhu, P. Wang, W. Qiu, Y. Liu, C. Ye, G. Fang, Y. Song, Appl. Phys. Lett. 78 (2001) 1319.

[102] Z. Tian, C. He, C. Liu, W. Yang, J. Yao, Y. Nie, Q. Gong, Y. Liu, Mater. Chem. Phys. 94 (2005) 444.

[103] J.J. Doyle, B. Ballesteros, G. de la Torre, D.A. McGovern, J.M. Kelly, T. Torres, W.J. Blau, Chem. Phys. Lett. 428 (2006) 307.

[104] Y. Song, G. Fang, Y. Wang, S. Liu, C. Li, L. Song, Y. Zhu, Q. Hu, Appl. Phys. Lett. 74 (1999) 332.

[105] Y. Liu, J. Zhou, X. Zhang, Z. Liu, X. Wan, J. Tian, T. Wang, Y. Chen, Carbon 47 (2009) 3113.

[106] A. Midya, V. Mamidala, J.-X. Yang, P.K.L. Ang, Z.-K. Chen, W. Ji, K.P. Loh, Small 6 (2010) 2292.

[107] X. Zhang, X. Yang, Y. Ma, Y. Huang, Y. Chen, J. Nanosci. Nanotechnol. 10 (2010) 2984.

[108] M.K. Kavitha, H. John, P. Gopinath, R. Philip, J. Mater. Chem. C 1 (2013) 3669.

[109] K. Erickson, R. Erni, Z. Lee, N. Alem, W. Gannett, A. Zettl, Adv. Mater. 22 (2010) 4467.

[110] W. Gao, L.B. Alemany, L. Ci, P.M. Ajayan, Nat. Chem. 1 (2009) 403.

[111] W. Cai, R.D. Piner, F.J. Stadermann, S. Park, M.A. Shaibat, Y. Ishii, D. Yang, A. Velamakanni, S.J. An, M. Stoller, J. An, D. Chen, R.S. Ruoff, Science 321 (2008) 1815.

[112] J.I. Paredes, S.V. Rodil, A.M. Alonso, J.M.D. Tascón, Langmuir 24 (2008) 10560.

[113] G.I. Titelman, V. Gelman, S. Bron, R.L. Khalfin, Y. Cohen, H.B. Peled, Carbon 43 (2005) 641.

[114] S.H. Dave, C. Gong, A.W. Robertson, J.H. Warner, J.C. Grossman, ACS Nano 10 (2016) 7515.

[115] T. Szabo, O. Berkesi, P. Forgo, K. Josepovits, Y. Sanakis, D. Petridis, I. Dekany, Chem. Mater. 18 (2006) 2740.

[116] A. Lerf, H.Y. He, M. Forster, J. Klinowski, J. Phys. Chem. B 102 (1998) 4477.

[117] T. Nakajima, A. Mabuchi, R. Hagiwara, Carbon 26 (1998) 357.

[118] H. He, J. Klinowski, M. Forster, A. Lerf, Chem. Phys. Lett. 287 (1998) 53.

[119] D.R. Dreyer, S. Park, C.W. Bielawski, R.S. Ruoff, Chem. Soc. Rev. 39 (2010) 228.

[120] K.P. Loh, Q. Bao, G. Eda, M. Chhowalla, Nature Chem. 2 (2010) 1015.

[121] G. Eda, C. Mattevi, H. Yamaguchi, H. Kim, M. Chhowalla, J. Phys. Chem. C 113 (2009) 15768.

[122] G. Eda, Y.Y. Lin, C. Mattevi, H. Yamaguchi, H.A. Chen, I.S. Chen, C.W. Chen, M. Chhowalla, Adv. Mater. 22 (2009) 505.

[123] S. Eigler, A. Hirsch, Angew. Chem. Int. Ed. 53 (2014) 7720.

[124] D.R. Dreyer., A.D. Todd, C.W. Bielawski, Chem. Soc. Rev. 43 (2014) 5288.

[125] V. Singh, D. Joung, L. Zhai, S. Das, S.I. Khondaker, S. Seal, Prog. Mater. Sci. 56 (2011) 1178.

[126] D. Chen, H. Feng, J. Li, Chem. Rev. 112 (2012) 6027.

[127] S. Stankovich, R.D. Piner, X.Q. Chen, N.Q. Wu, S.R. Nguyen, R.S. Ruoff, J. Mater. Chem. 16 (2006) 155.

[128] S. Stankovich, D.A. Dikin, R.D. Piner, K.A. Kohlhaas, A. Kleinhammes, Y. Jia, Y. Wu, S. Binh, T. Nguyen, R.S. Ruoff, Carbon 45 (2007) 1558.

[129] M.J. Fernández-Merino, L. Guardia, J.I. Paredes, S. Villar-Rodil, P. Solís-Fernández, A. Martínez-Alonso, J.M.D. Tascón, J. Phys. Chem. C 114 (2010) 6426.

[130] C. Mattevi, G. Eda, S. Agnoli, S. Miller, K.A. Mkhoyan, O. Celik, D. Mastrogiovanni, G. Granozzi, E. Garfunkel, M. Chhowalla, Adv. Funct. Mater. 19 (2009) 2577.

[131] I. Jung, D.A. Dikin, R.D. Piner, R.S. Ruoff, Nano Lett. 8 (2008) 4283.

[132] A. Mathkar, D. Tozier, P. Cox, P. Ong, C. Galande, K. Balakrishnan, A.L.M. Reddy, P.M. Ajayan, J. Phys. Chem. Lett. 3 (2012) 8.

[133] C. Gómez-Navarro, J.C. Meyer, R.S. Sundaram, A. Chuvilin, S. Kurasch, M. Burghard, K. Kern, U. Kaiser, Nano Lett. 10 (2010) 1144.

[134] S.F. Pei, H.M. Cheng, Carbon 50 (2012) 3210.

[135] S. Mao, H.H. Pu, J.H. Chen, RSC Adv. 2 (2012) 2643.

[136] Z. Liu, Y. Wang, X. Zhang, Y. Xu, Y. Chen, J. Tian, Appl. Phys. Lett. 94 (2009) 021902.

[137] B. Zhao, B. Cao, W. Zhou, D. Li, W. Zhao, J. Phys. Chem. C 114 (2010) 12517.

[138] X.F. Jiang, L. Polavarapu, H. Zhu, R. Ma, Q.H. Xu, Photon. Res. 3 (2015) A87.

[139] G.K. Lim, Z.L. Chen, J. Clark, R.G.S. Goh, W.H. Ng, H.W. Tan, R.H. Friend, P.K.H. Ho, L.L. Chua, Nature Photonics 5 (2011) 554.

[140] N. Liaros, K. Iliopoulos, M.M. Stylianakis, E. Koudoumas, S. Couris, Opt. Mater. 36 (2014) 112.

[141] X.L. Zhang, Z.B. Liu, X.Q. Yan, X.C. Li, Y.S. Chen, J.G. Tian, J. Opt. 17 (2015) 015501.

[142] X.L. Zhang, Z.B. Liu, X.C. Li, Q. Ma, X.D. Chen, J.G. Tian, Y.F. Xu, Y.S. Chen, Opt. Express 21 (2013) 7511.

[143] V. Georgakilas, M. Otyepka, A.B. Bourlinos, V. Chandra, N. Kim, K.C. Kemp, P. Hobza, R. Zboril, K.S. Kim, Chem. Rev. 112 (2012) 6156.

[144] B.I. Kharisov, O.V. Kharissova, A.V. Dimas, I.G. de la Fuente, Y. Peña Méndez, J. Coord. Chem. 69 (2016) 1125.

[145] Y. Chen, T. Bai, N. Dong, F. Fan, S. Zhang, X. Zhuang, J. Sun, B. Zhang, X. Zhang, J. Wang, W.J. Blau, Prog. Mater. Sci. 84 (2016) 118.

[146] R.K. Layek, A.K. Nandi, Polymer 54 (2013) 5087.

[147] K.P. Loh, Q. Bao, P.K. Ang, J. Yang, J. Mater. Chem. 20 (2010) 2277.

[148] X.L. Zhang, X. Zhao, Z.B. Liu, Y.S. Liu, Y.S. Chen, J.G. Tian, Opt. Express 17 (2009) 23959.

[149] M. Feng, R. Sun, H. Zhan, Y. Chen, Carbon 48 (2010) 1177.

[150] Y. Wang, M. Lv, J. Guo, T. Wang, J. Shao, D. Wang, Y.W. Yang, Sci. China Chem. 58 (2015) 1782.

[151] J. Wang, Y. Chen, R. Li, H. Dong, L. Zhang, M. Lotya, J.N. Coleman, W.J. Blau, Carbon Nanotubes - Synthesis, Characterization, Applications, S. Yellampalli (Ed.), InTech, Rijeka, Croatia, 2011.

[152] Z. Liu, X.L. Zhang, X.Q. Yan, Y.S. Chen, J.G. Tian, Chin. Sci. Bull. 57 (2012) 2971.

[153] A. Wang, L. Long, W. Zhao, Y. Song, M.G. Humphrey, M.P. Cifuentes, X. Wu, Y. Fu, D. Zhang, X. Li, C. Zhanga, Carbon 53 (2013) 327.

[154] A. Wang, W. Yu, Z. Xiao, Y. Song, L. Long, M.P. Cifuentes, M.G. Humphrey, C. Zhang, Nano Res. 8 (2015) 870.

[155] W. Song, C. He, Y. Dong, W. Zhang, Y. Gao, Y. Wu, Z. Chen, Phys. Chem. Chem. Phys. 17 (2015) 7149.

[156] R. Yamuna, S. Ramakrishnan, K. Dhara, R. Devi, N.K. Kothurkar, E. Kirubha, P.K. Palanisamy, J. Nanopart. Res. 15 (2013) 1399.

[157] K. Garg, R. Shanmugam, P.C. Ramamurthy, Carbon 122 (2017) 307.

[158] G.J. Zhou, W.Y. Wong, D. Cui, C. Ye, Chem. Mater. 17 (2005) 5209.

[159] M.B.M. Krishna, V.P. Kumar, N. Venkatramaiah, R. Venkatesan, D.N. Rao, Appl. Phys. Lett. 98 (2011) 081106.

[160] M.B.M. Krishna, N. Venkatramaiah, R. Venkatesan, D.N. Narayana, J. Mater. Chem. 22 (2012) 3059.

[161] M.B.M. Krishna, N. Venkatramaiah, D.N. Rao, J. Opt. 16 (2013) 015205.

[162] A. Wang, J. Song, D. Jia, W. Yu, L. Long, Y. Song, M.P. Cifuentes, M.G. Humphrey, L. Zhang, J. Shao, C. Zhang, Inorg. Chem. Front. 3 (2016) 296.

[163] A. Wang, W. Yu, Z. Huang, F. Zhou, J. Song, Y. Song, L. Long, M.P. Cifuentes, M.G. Humphrey, L. Zhang, J. Shao, C. Zhang, Sci. Rep. 6 (2016) 23325.

[164] Y. Du, N. Dong, M. Zhang, K. Zhu, R. Na, S. Zhang, N. Sun, G. Wang, J. Wang, Phys. Chem. Chem. Phys. 19 (2017) 2252.

[165] J. Zhu, Y. Li, Y. Chen, J. Wang, B. Zhang, J. Zhang, W.J. Blau, Carbon 49 (2011) 1900.

[166] X. Zhao, X.Q. Yan, Q. Ma, J. Yao, X.L. Zhang, Z.B. Liu, J.G. Tian, Chem. Phys. Lett. 577 (2013) 62.

[167] Y.X. Li, J.H. Zhu, Y. Chen, J.J. Zhang, J. Wang, B. Zhang, Y. He, W.J. Blau, Nanotechnology 22 (2011) 205704.

[168] W. Song, C. He, W. Zhang, Y. Gao, Y. Yang, Y. Wu, Z. Chen, X. Li, Y. Dong, Carbon 77 (2014) 1020.

[169] Z. Wang, C. He, W. Song, Y. Gao, Z. Chen, Y. Dong, C. Zhao, Z. Liu, Y. Wu, RSC Adv. 5 (2015) 94144.

[170] Z. Li, C. He, Z. Wang, Y. Gao, Y. Dong, C. Zhao, Z. Chen, Y. Wu, W. Song, Photochem. Photobiol. Sci. 15 (2016) 910.

[171] E. Jiang, C. He, X. Xiao, Y. Dong, Y. Gao, Z. Chen, Y. Wu, W. Song, Opt. Mater. 64 (2017) 193.

[172] G. Grelaud, M.P. Cifuentes, F. Paul, M.G. Humphrey, J. Organomet. Chem. 751 (2014) 181.

[173] A. Barlow, PhD Thesis, Australian National University, Australia, 2014.

[174] R. Liu, J. Hu, S. Zhu, J. Lu, H. Zhu, ACS Appl. Mater. Interfaces 9 (2017) 33029.

Figure Captions

Figure 1. Passive optical limiting for sensor protection with different laser intensities.

Figure 2. Schematic output vs input fluence plot showing optical limiting response of an ideal optical limiter.

Figure 3. Five-level Jablonski diagram showing some NLA effects.

Figure 4. Open- and closed-aperture Z-scan experimental set-up.

Figure 5. Representative open-aperture Z-scan transmittance traces for: a) saturable absorption (SA), b) two-photon absorption (2PA), and c) reverse saturable absorption (RSA). Representative closed-aperture Z-scan transmittance traces for: d) self-defocusing and e) self-focusing.

Figure 6. Schematic structures of a) graphene oxide (GO) and b) reduced graphene oxide (RGO).

Figure 7. Schematic structure of reduced graphene oxide (RGO) showing sp^2 and sp^3 regions.

Figure 8. Schematic structure of **1**.

Figure 9. Schematic structure of **2**.

Figure 10. Schematic structures of **3**-**5**.

Figure 11. Schematic structure of **6** (M = Cu, Zn, VO, Sn).

Figure 12. Schematic structures of a) **7** and b) **8**.

Figure 13. Syntheses of **9** (two-step procedure) and **10** (**9** has a higher degree of TPP incorporation).

Figure 14. Schematic structures of a) **11** and b) **12**.

Figure 15. Schematic structures of a) **13** and b) **14**.

Figure 16. Schematic structure of **15**.

Figure 17. Schematic structure of **16**.

Figure 18. Schematic structure of **17**.

Figure 19. Schematic structures of a) **18** and b) **19**.

Figure 20. Schematic structure of **20** (M = Cu, Pb).

Figure 21. Schematic structures of a) **21** and b) **22**.

Figure 22. Schematic structures of a) **23** and b) **24**.

Figure 23. Schematic structures of a) **25** and b) **26**.

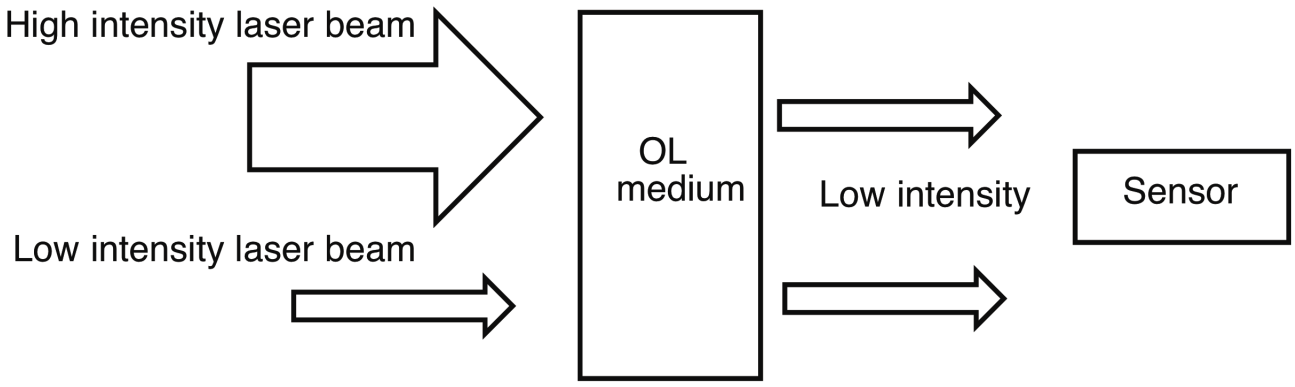
High intensity laser beam
Low intensity laser beam
OL
medium
Low intensity
Sensor

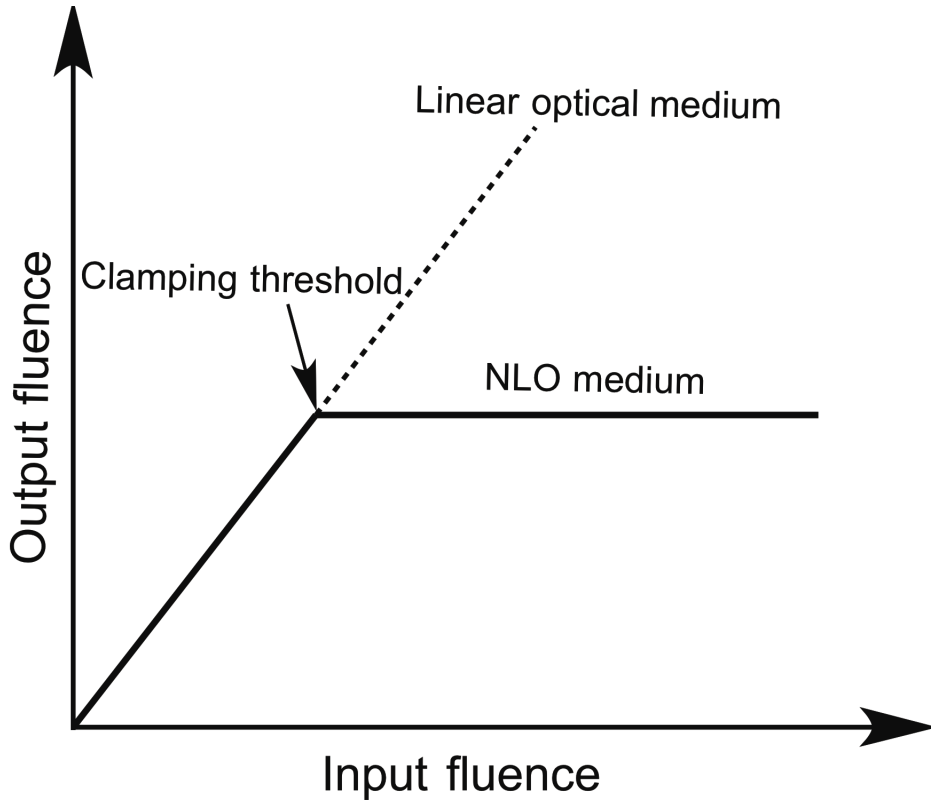
Linear optical medium
Clamping threshold
NLO medium
Output fluence
Input fluence

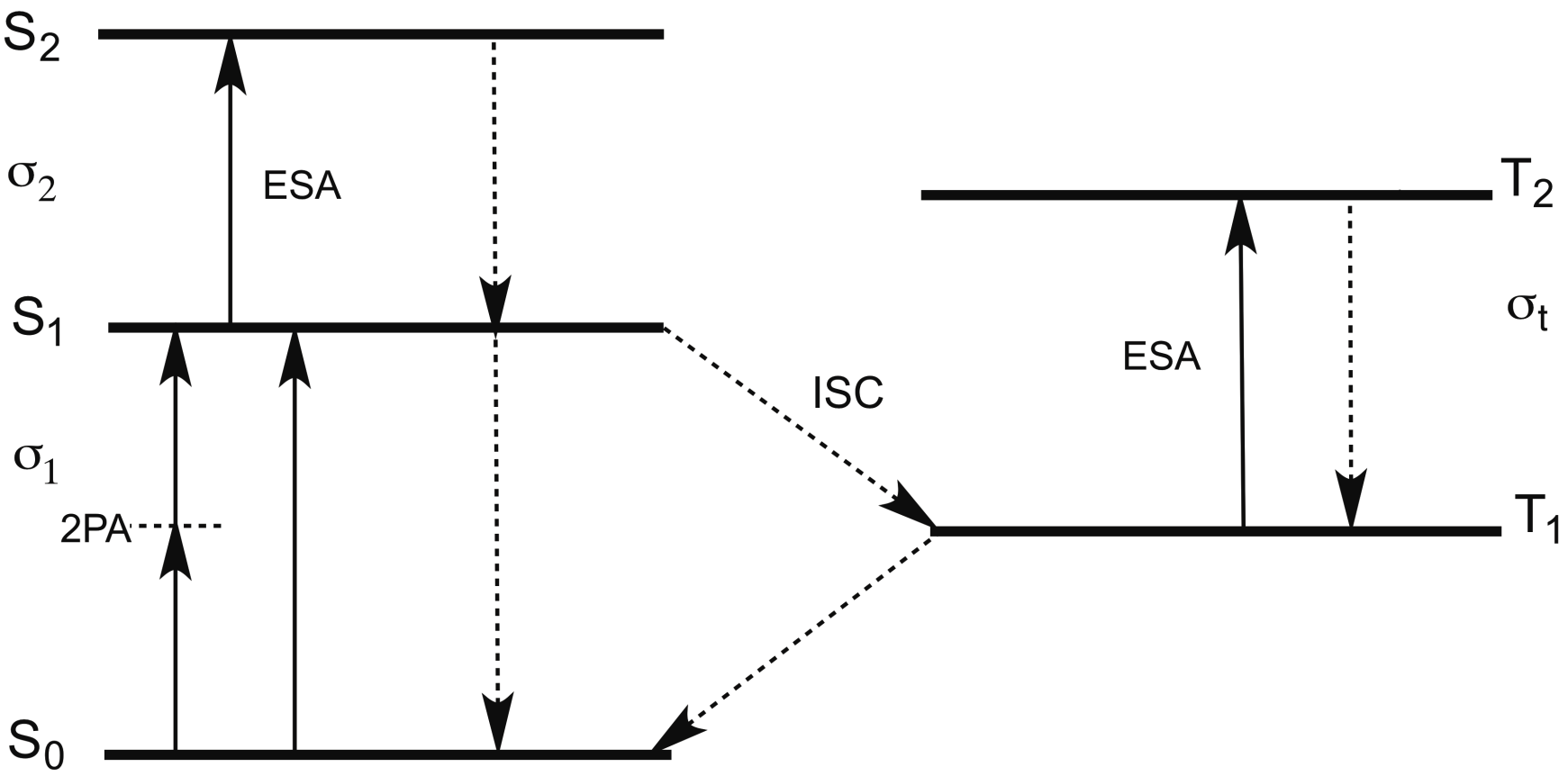
S2
σ2
ESA
S1
σ1
2PA
S0
ISC
T2
σt
ESA
T1

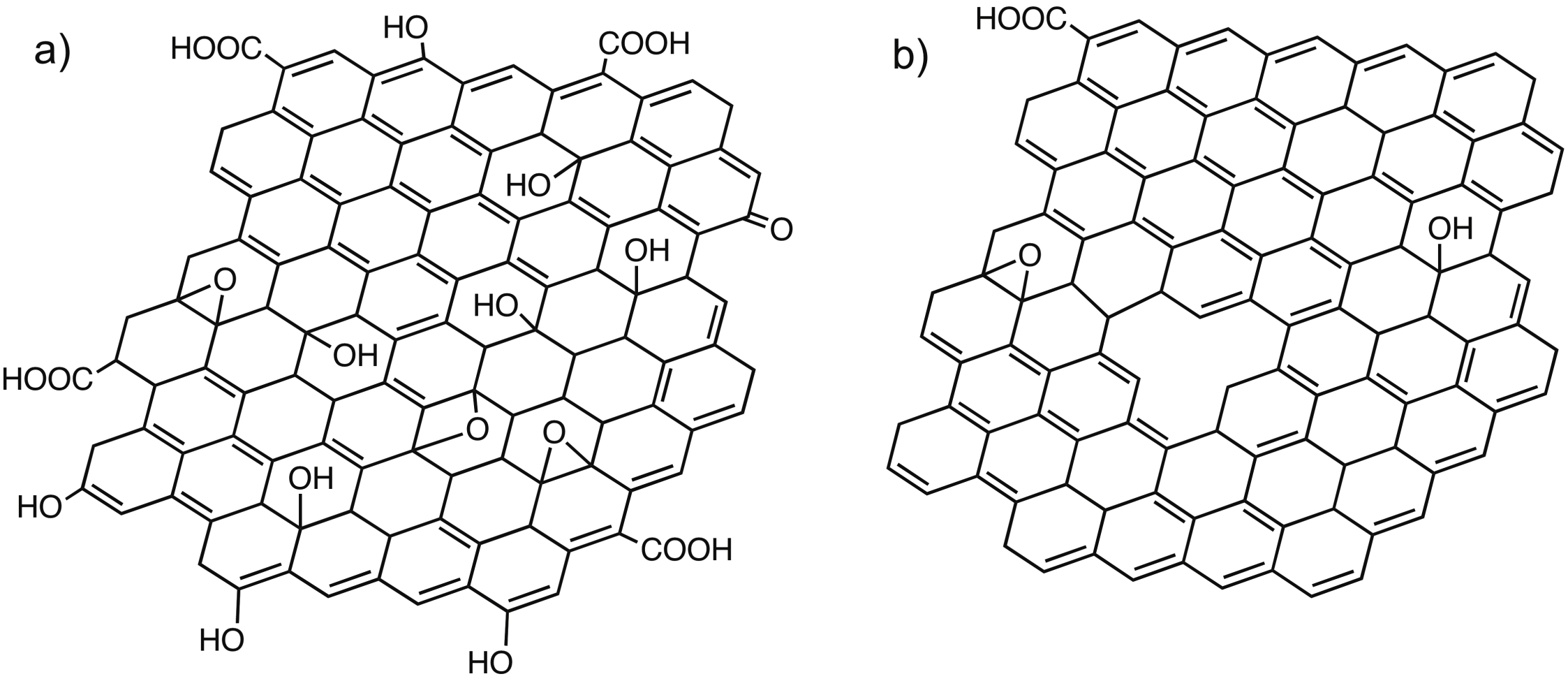
a)
HOOC
HO
COOH
HO
O
OH
O
HO
OH
HOOC
O
O
O
OH
HO
COOH
HO
HO
b)
HOOC
OH
O

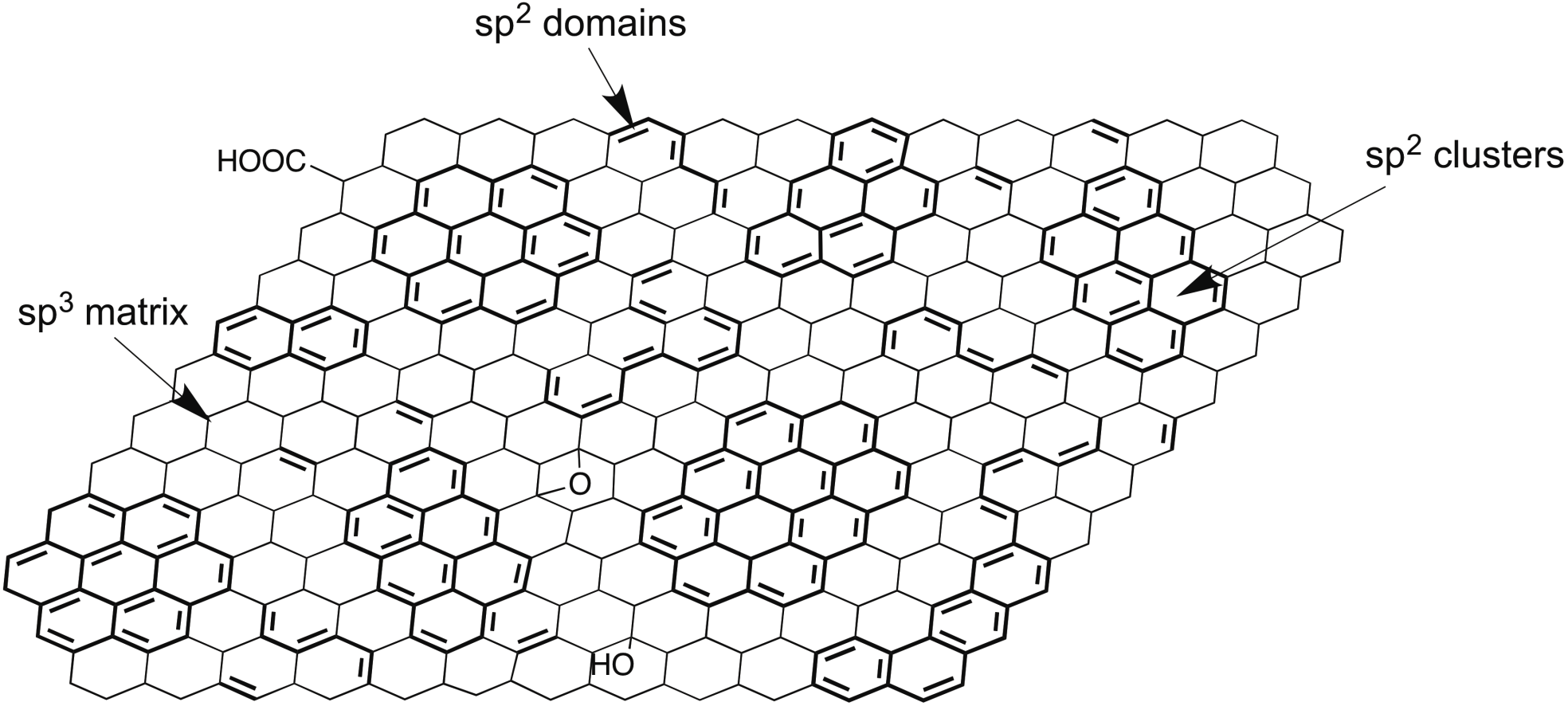
sp2 domains
HOOC
sp2 clusters
sp3 matrix
O
HO

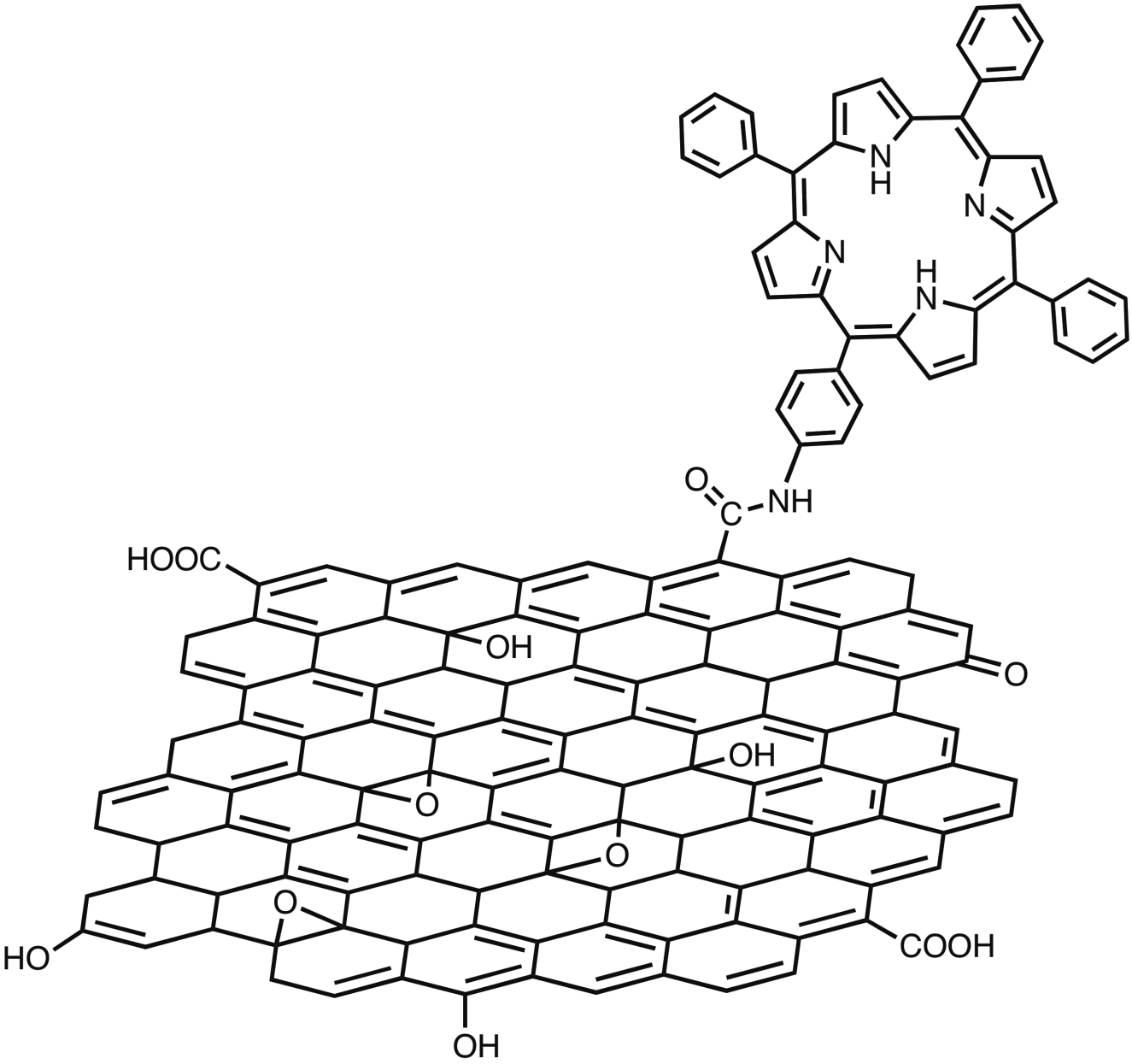
HOOC
OH
O
OH
O
O
O
HO
COOH
OH
O
C
NH
N
H
N
N
H
N

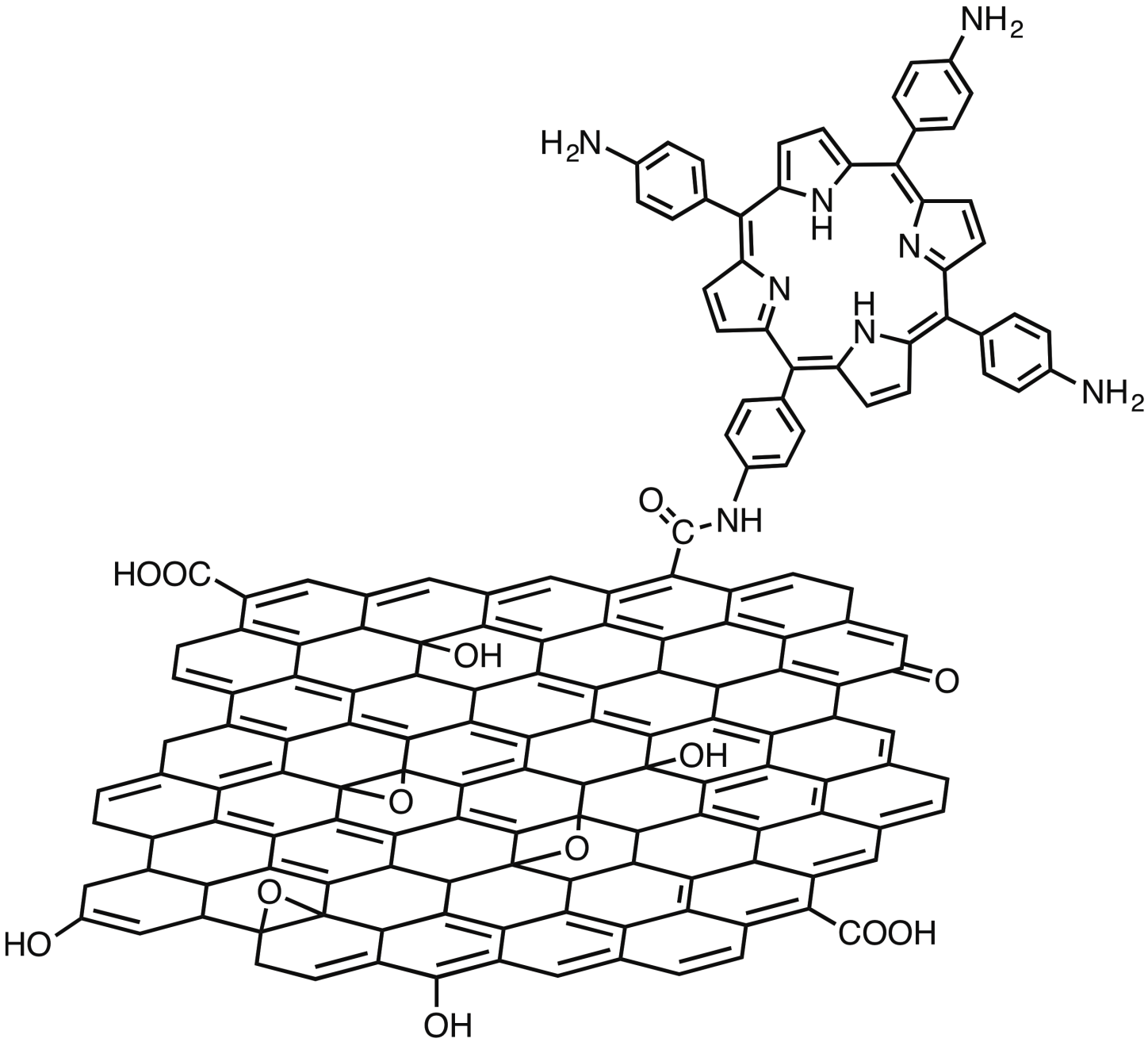
NH2
H2N
N
H
N
N
H
N
NH2
O
C
NH
HOOC
OH
O
OH
O
O
O
HO
COOH
OH

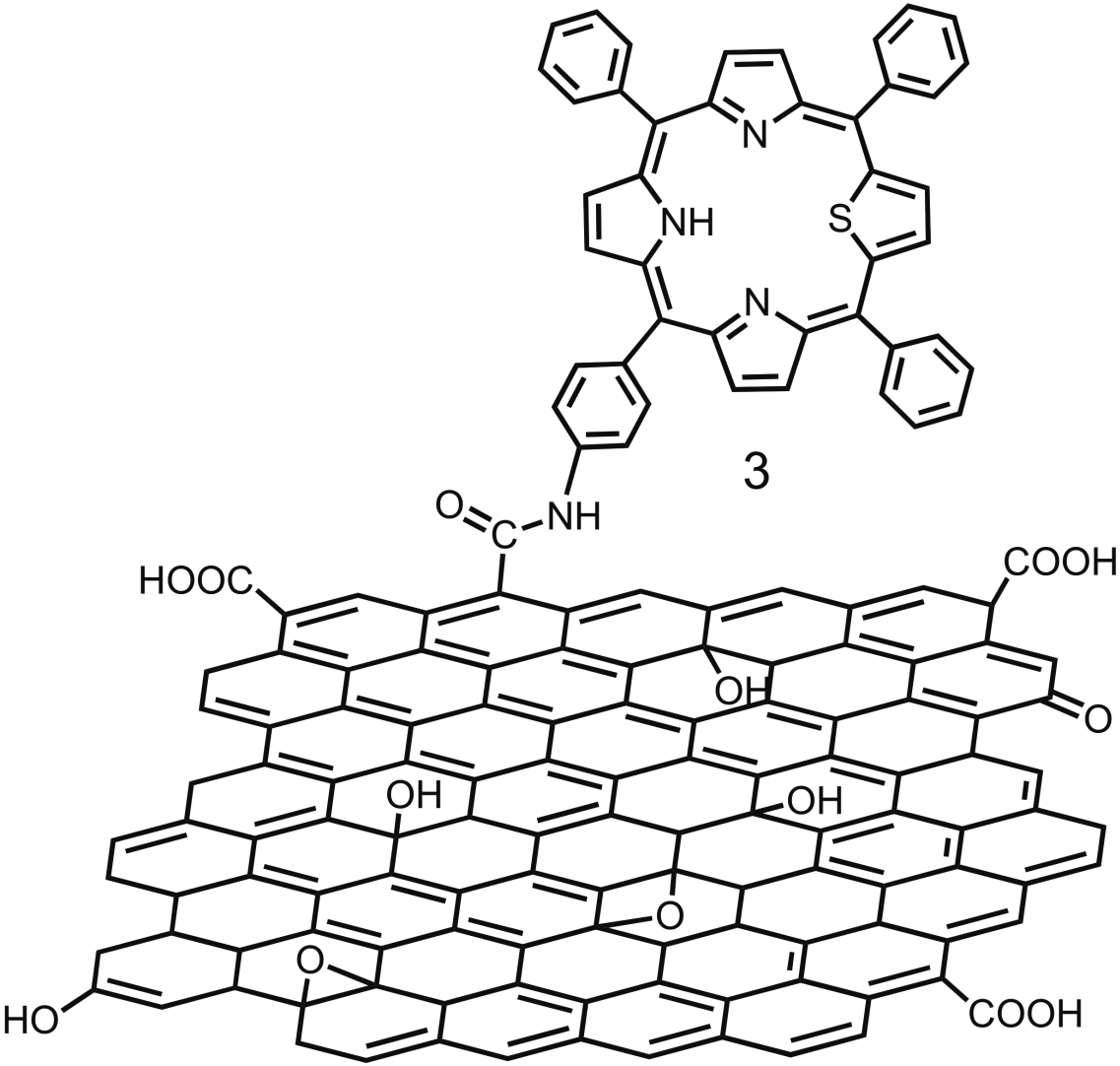

3

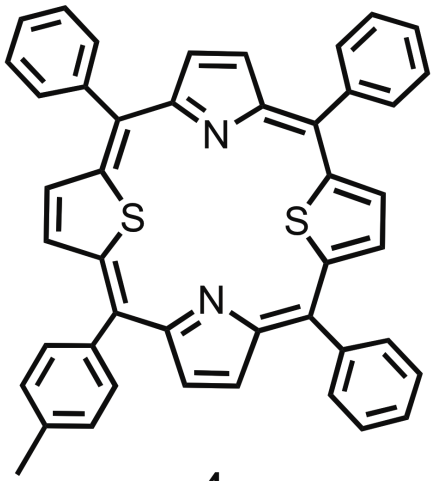

4

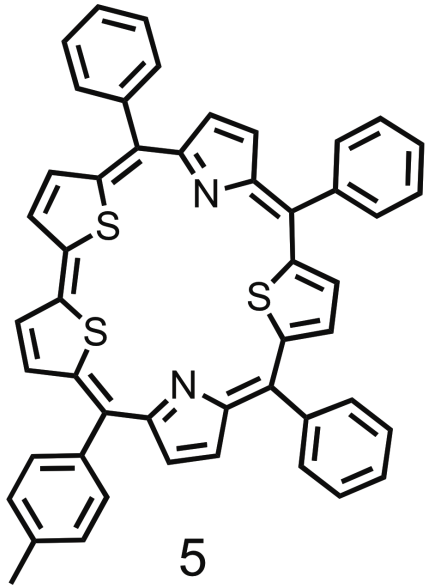

5

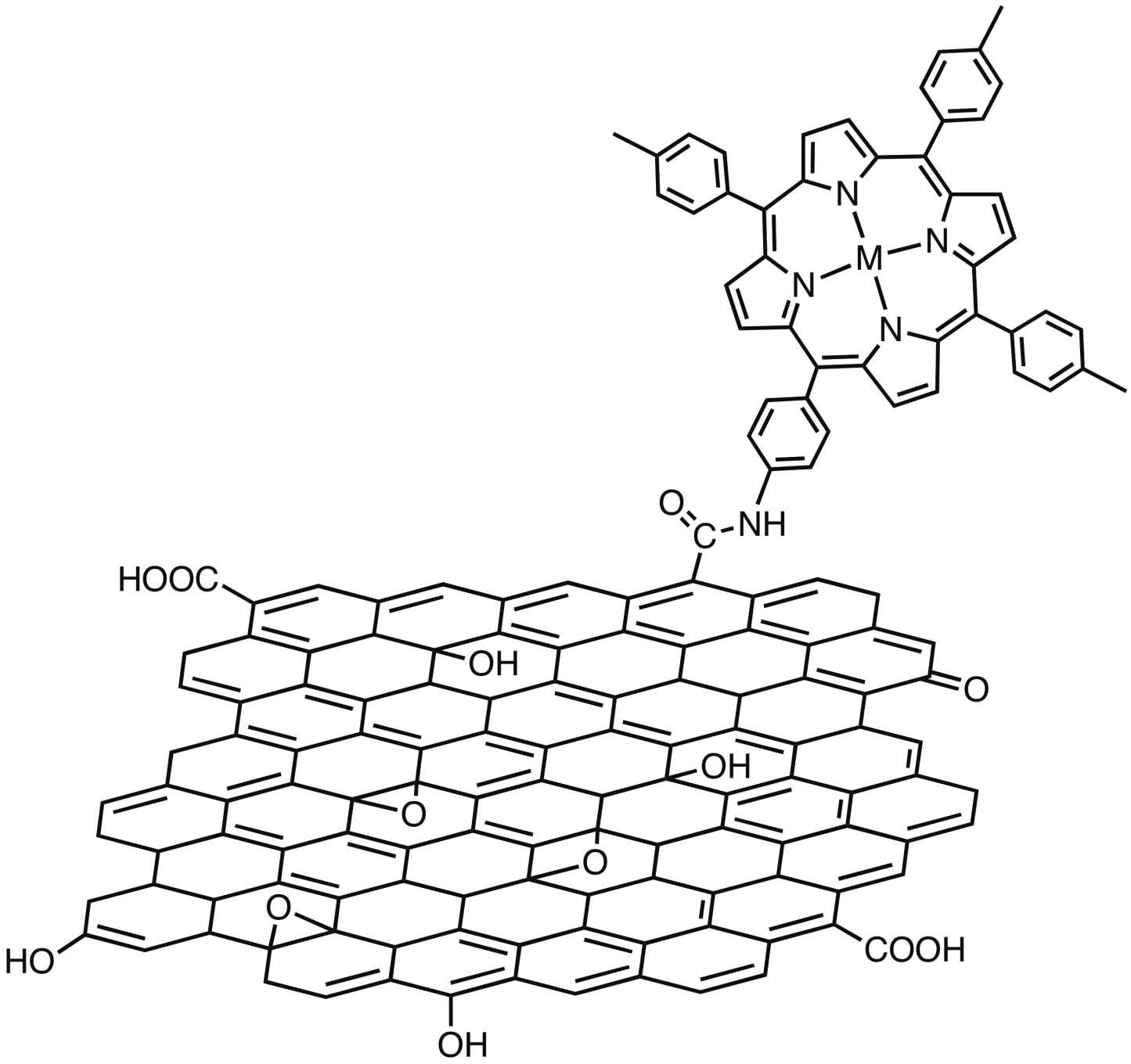
N
M
N
N
N
O
C
NH
HOOC
OH
O
OH
O
O
O
HO
COOH
OH

a)

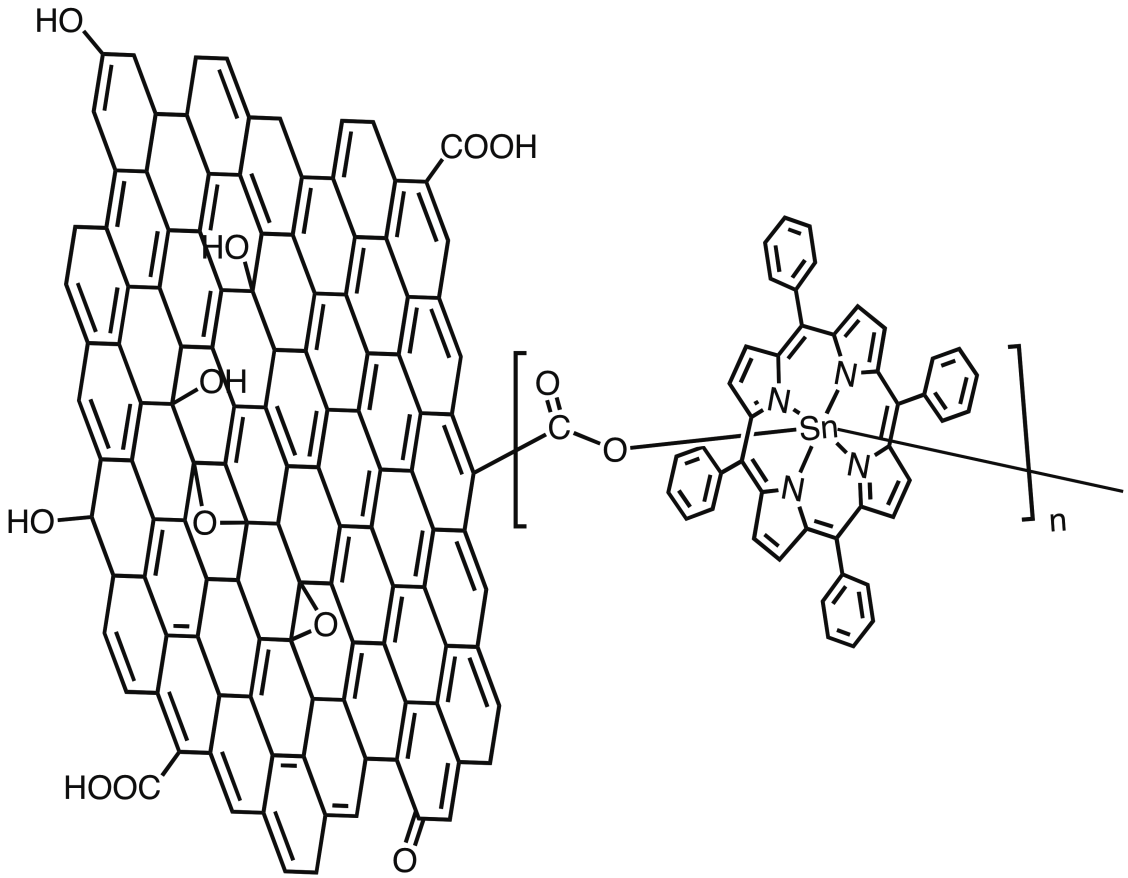
HO
COOH
HO
OH
HO
O
O
HOOC
O
O
C
O
N
N
Sn
N
N
n

b)

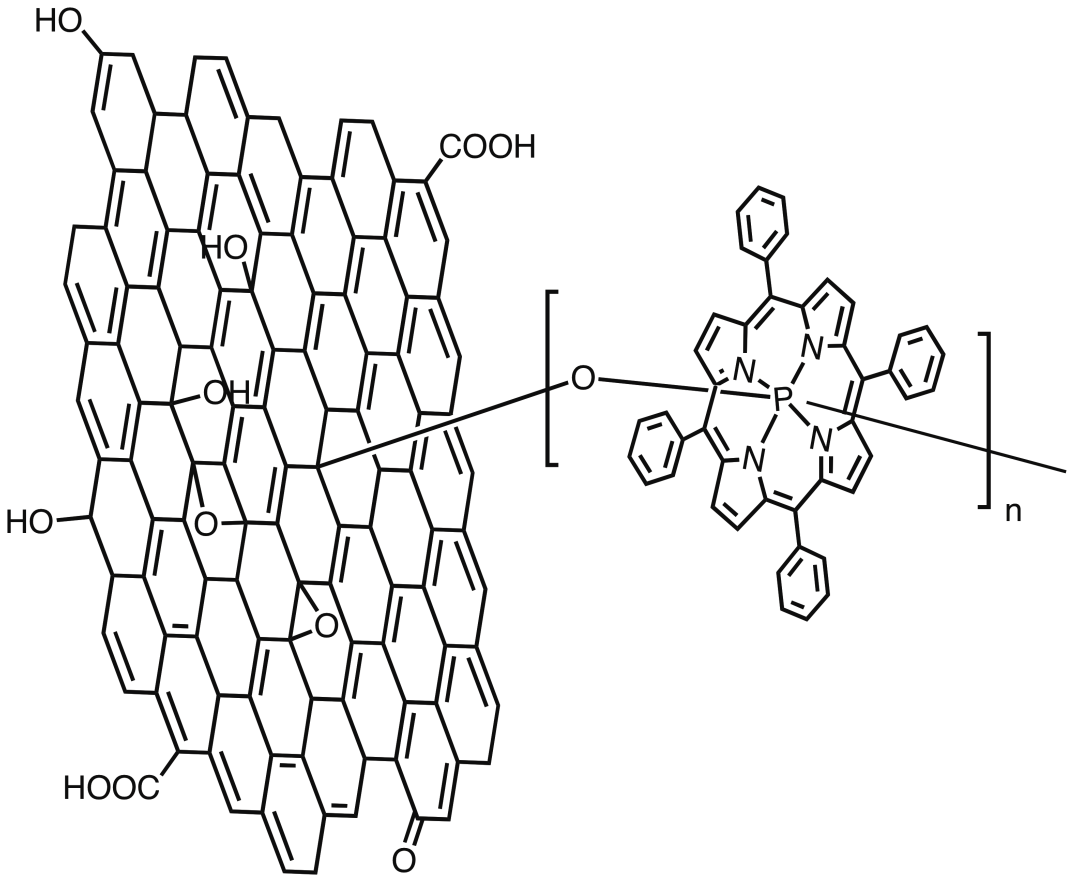
HO
COOH
HO
OH
HO
O
O
HOOC
O
O
N
N
P
N
N
n

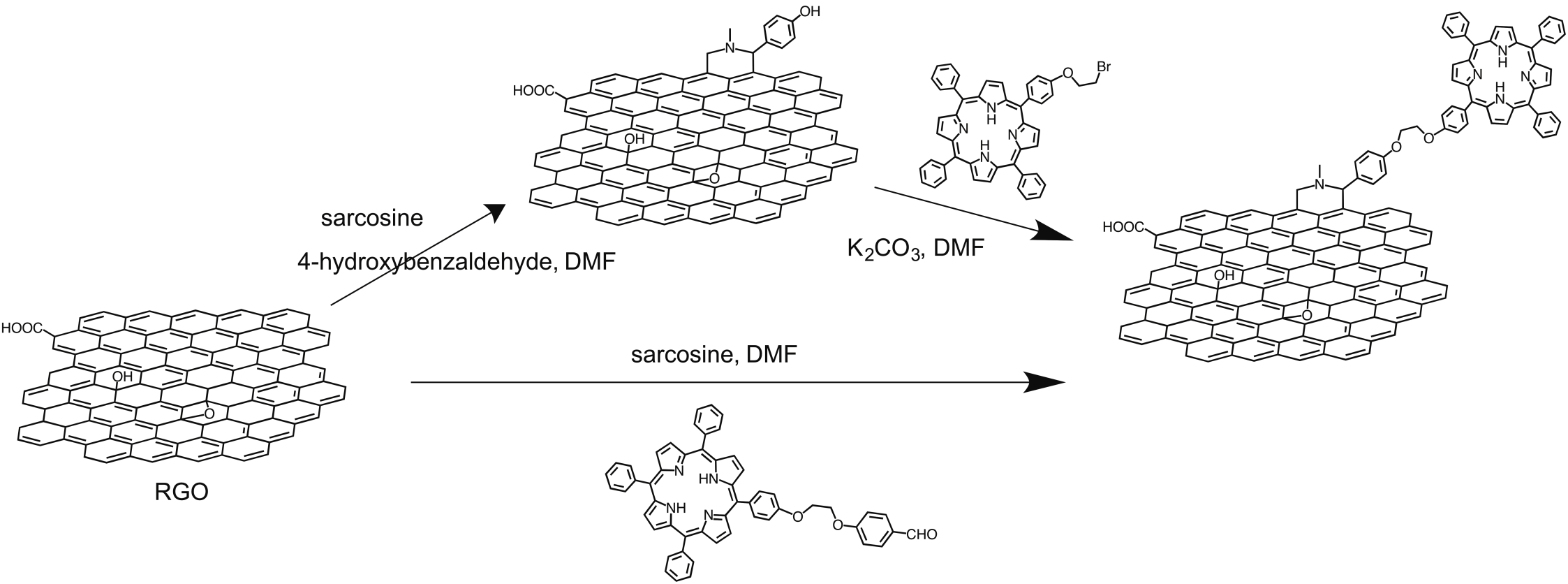
HOOC
OH
O
RGO
sarcosine
4-hydroxybenzaldehyde, DMF
HOOC
OH
OH
O
N
OH
K_2CO_3, DMF
Br
O
N
H
N
H
N
sarcosine, DMF
HN
NH
N
O
O
CHO
HOOC
OH
O
N
O
O
N
H
N
H
N

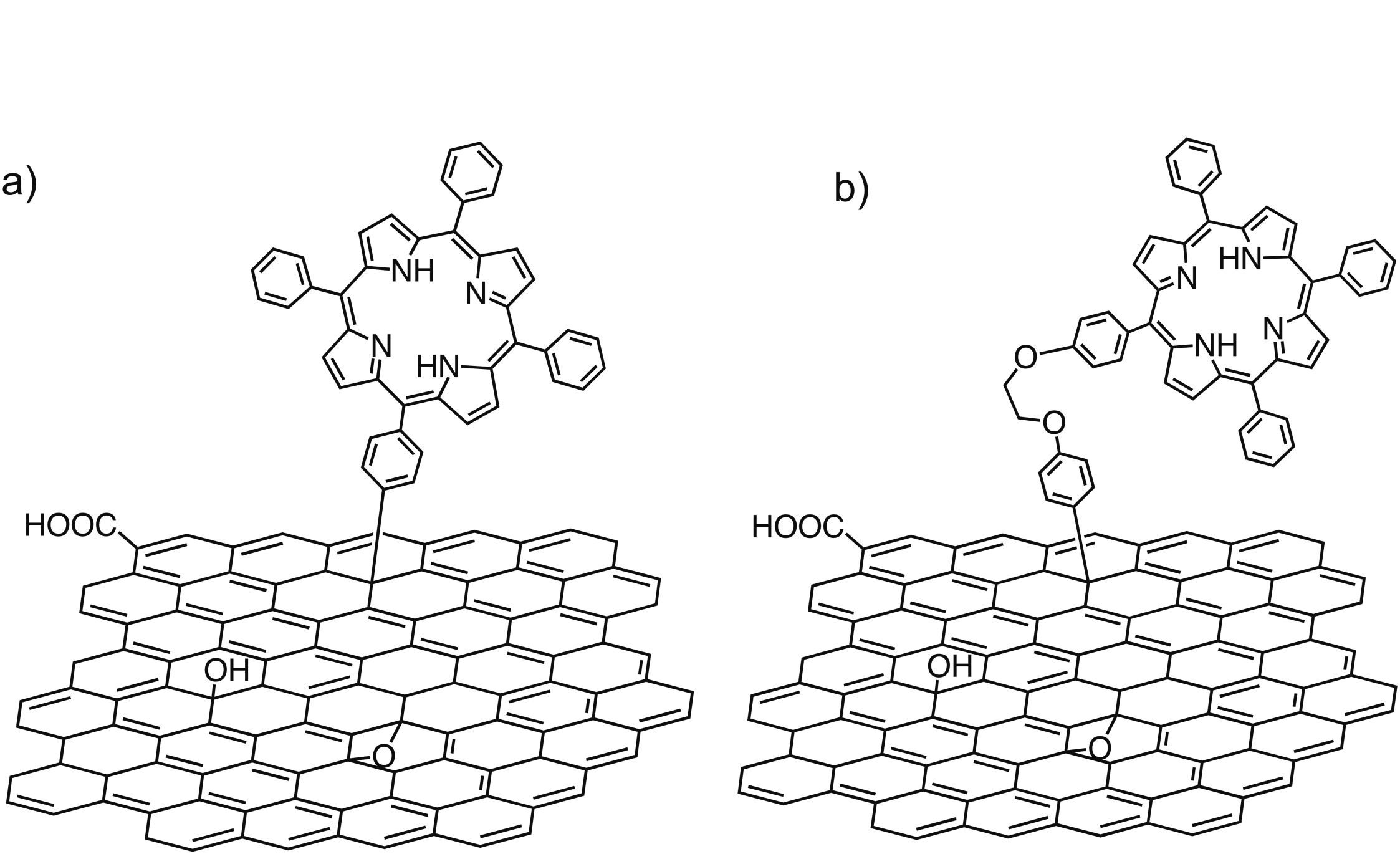
a)
NH
N
N
HN
HOOC
OH
O
b)
HN
N
NH
N
O
O
HOOC
OH
O

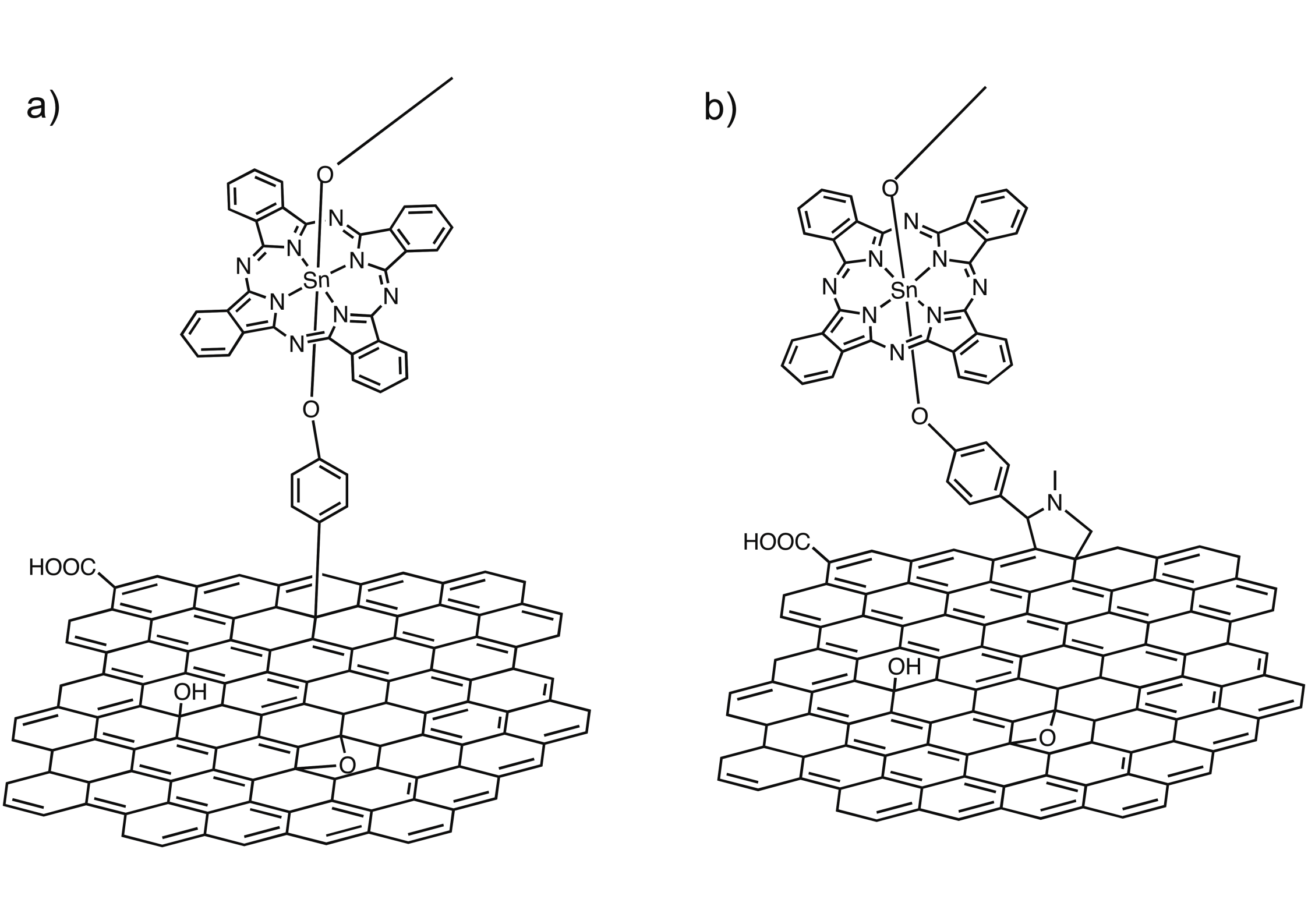
a)
b)
Sn
N
O
HOOC
OH
I

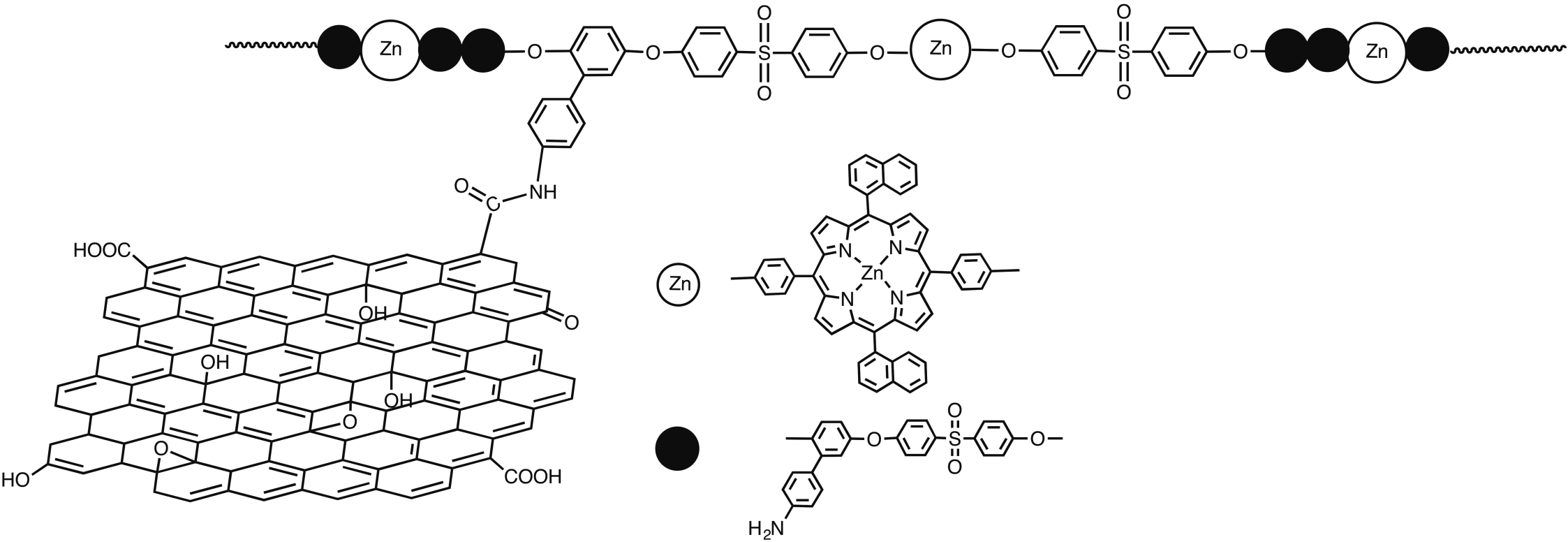
Zn
O
S
NH
HOOC
OH
HO
COOH
N
Zn
H_2N

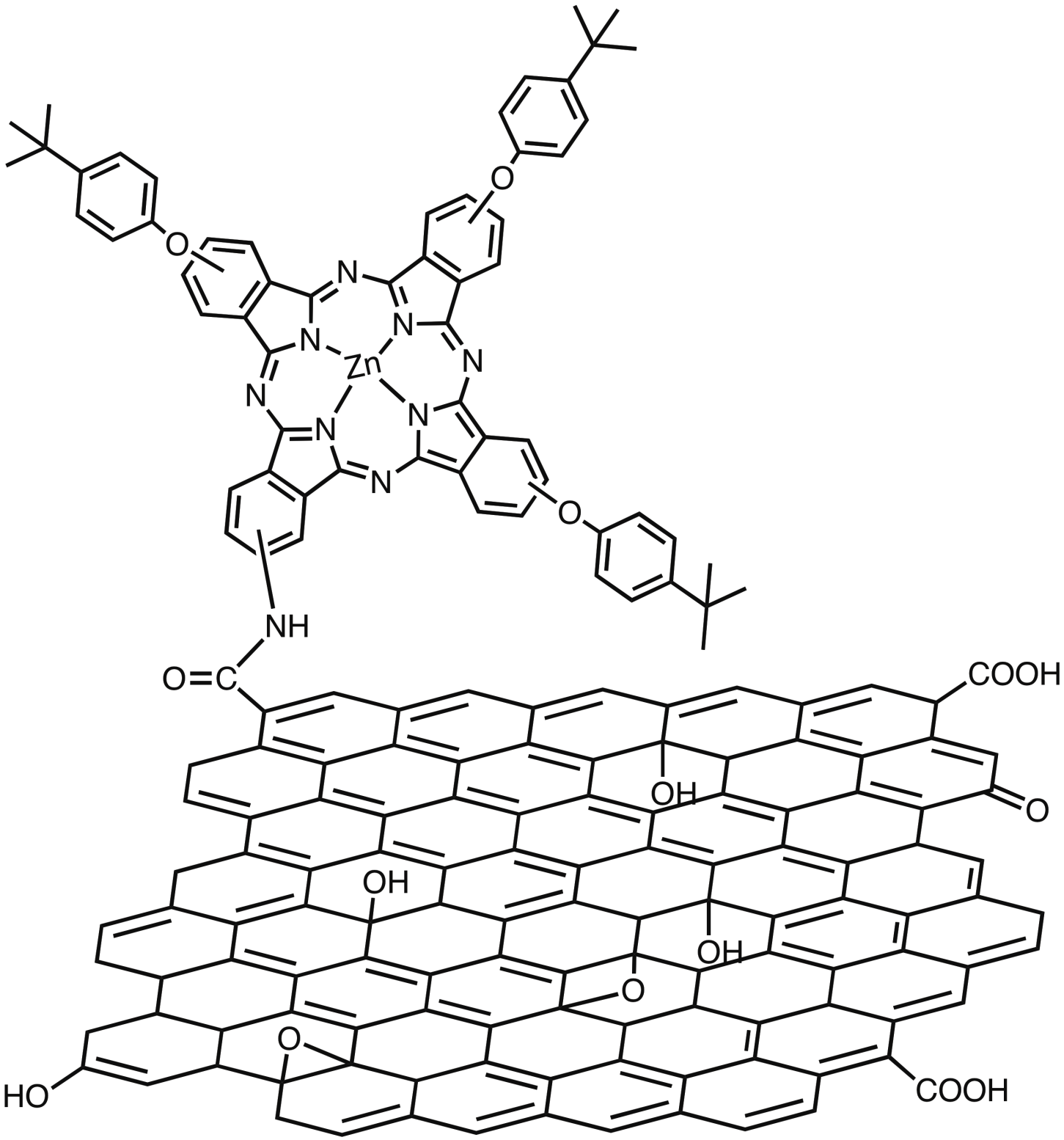
N
N
N
N
N
N
N
N
Zn
O
O
O
NH
O=C
COOH
OH
O
OH
OH
O
O
HO
COOH

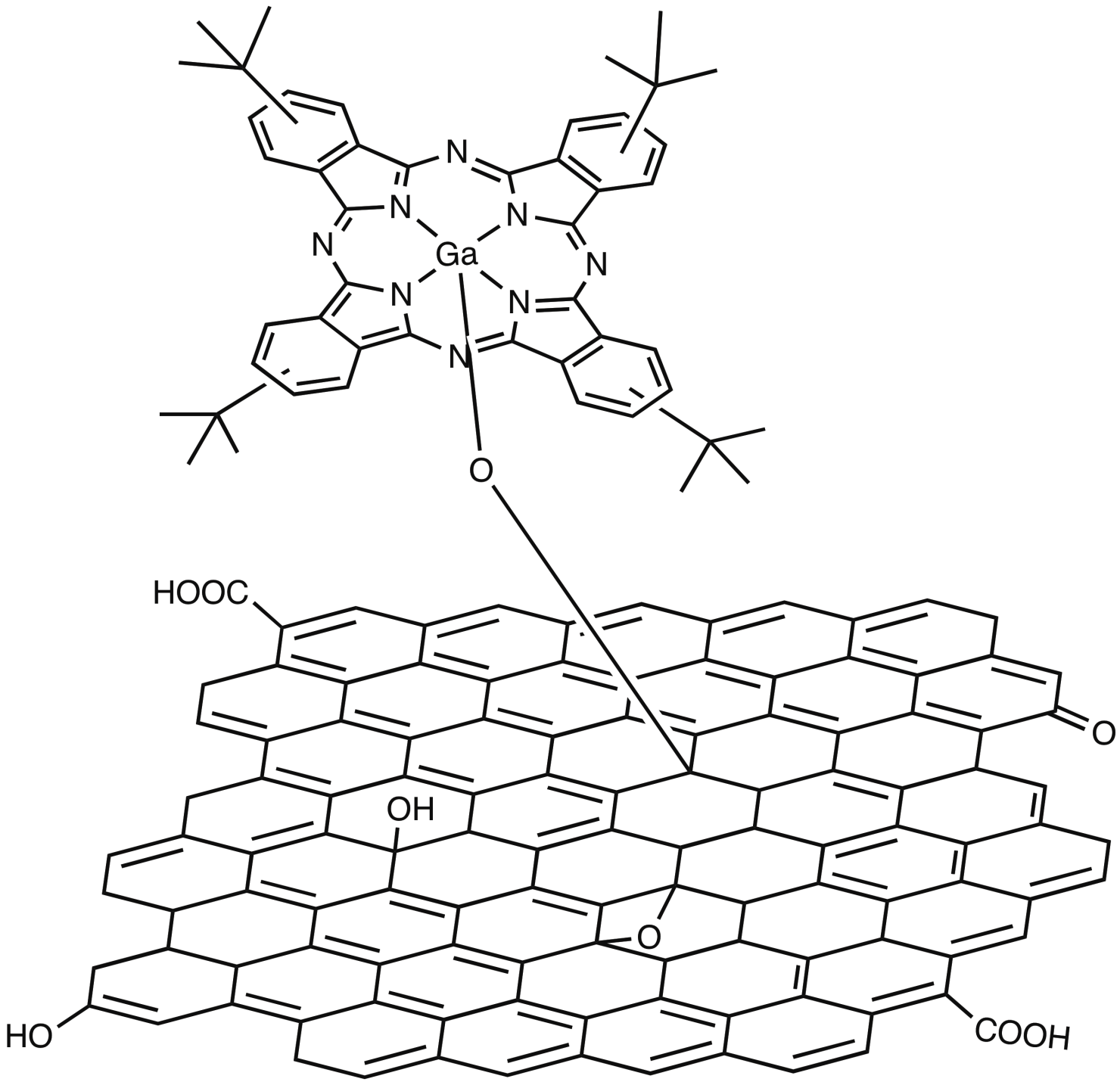
N
N
N
N
N
N
N
N
Ga
O
HOOC
O
OH
O
HO
COOH

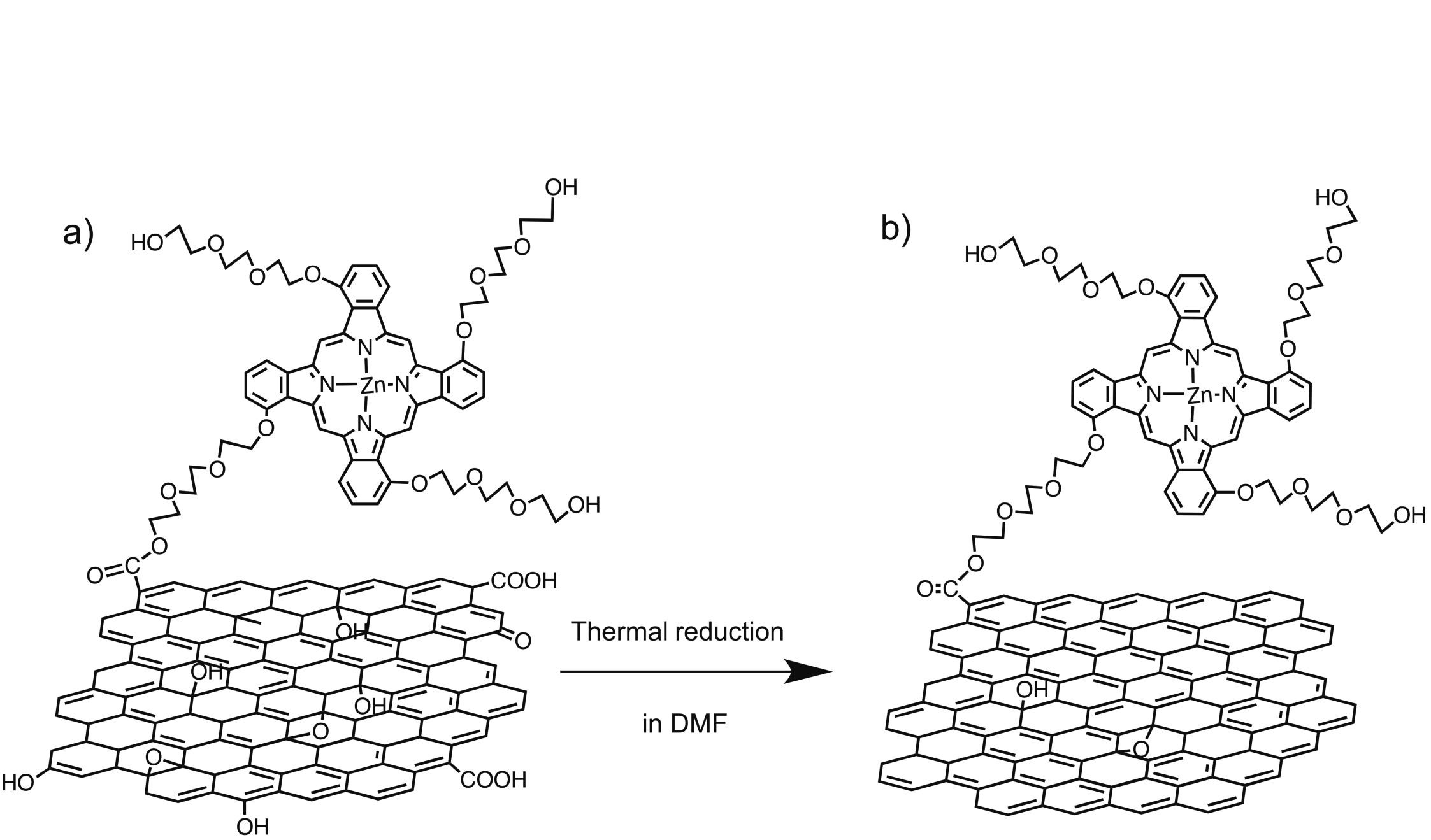
a)
b)
Thermal reduction
in DMF

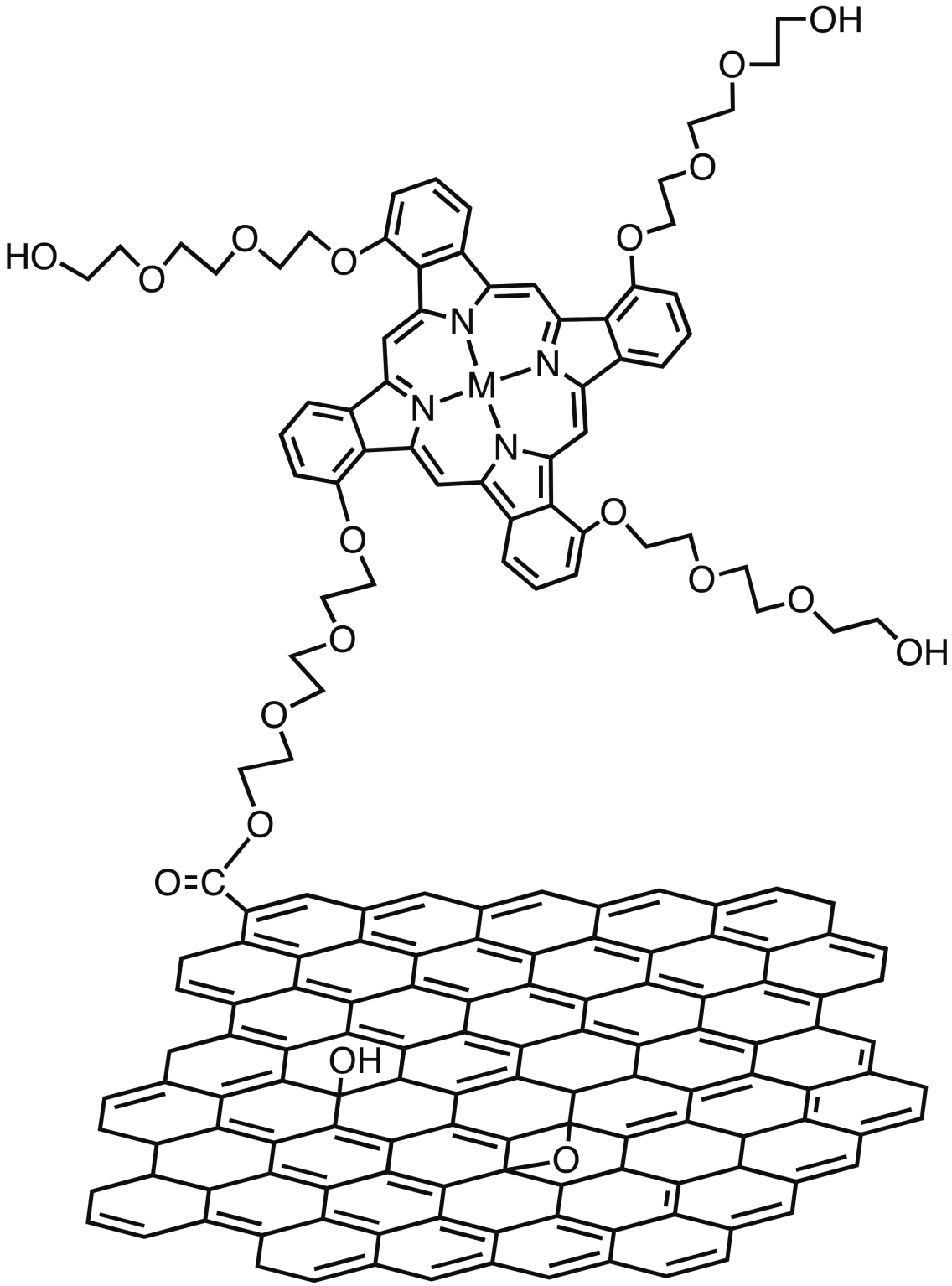
OH
O
O
O
HO
O
O
O
O
N
N
M
N
N
O
O
O
O
O
O
OH
O
O
O
O=C
OH
O

a)

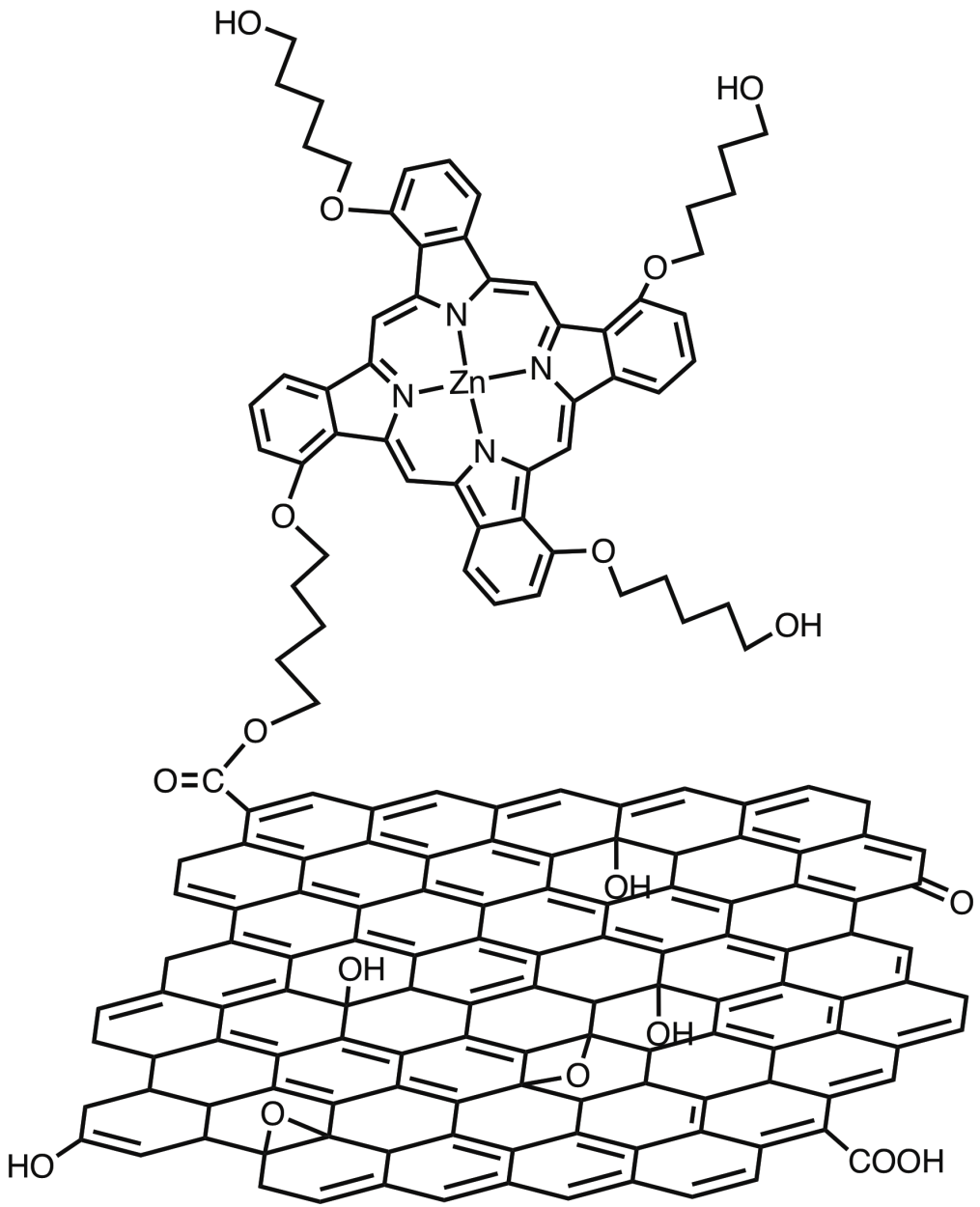
HO
HO
O
O
O
N
N
Zn
N
N
O
O
OH
O
O=C
OH
O
OH
OH
O
O
HO
COOH

b)

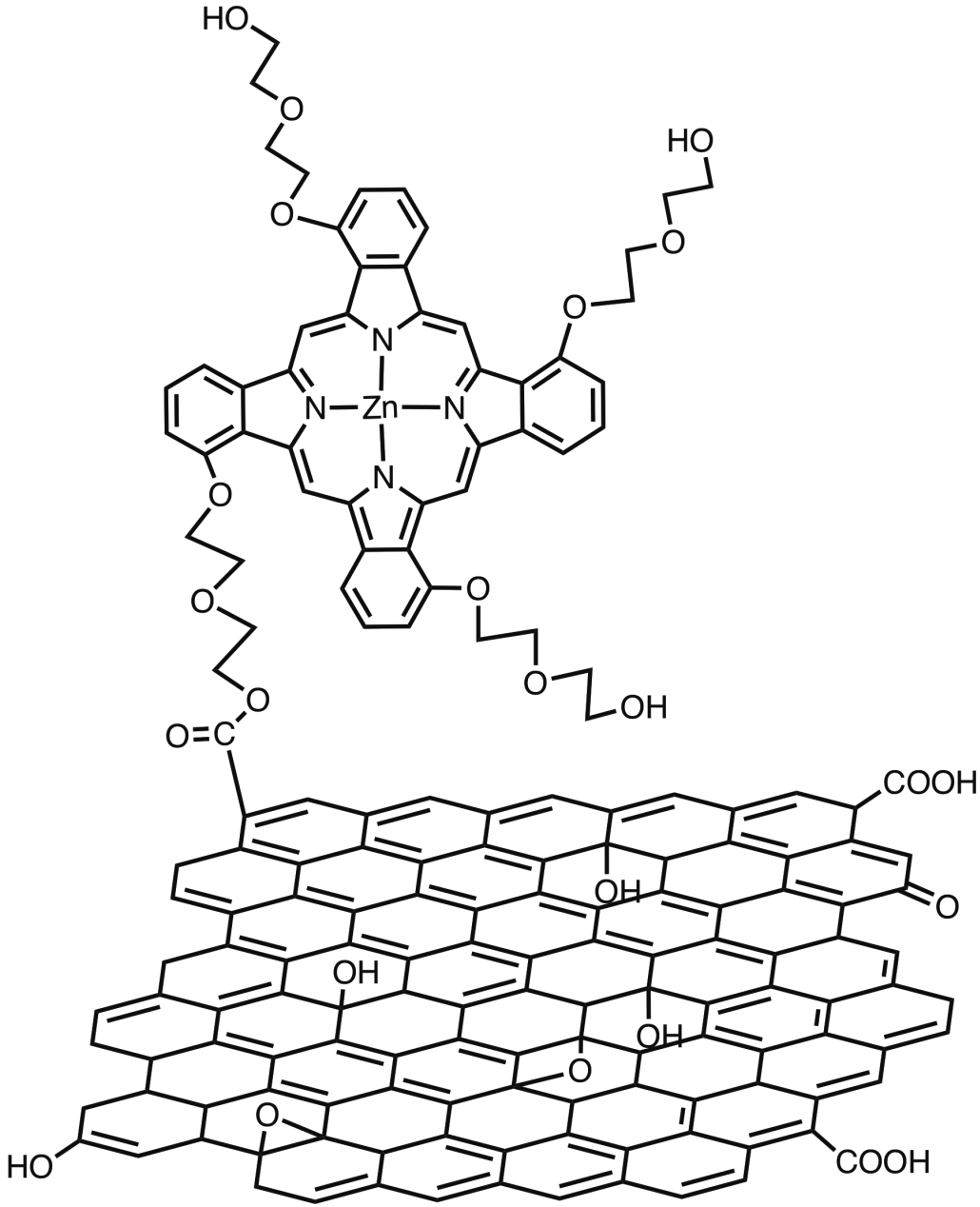
HO
O
O
HO
O
O
N
N
Zn
N
N
O
O
O
O
OH
O=C
O
COOH
OH
O
OH
OH
O
O
HO
COOH

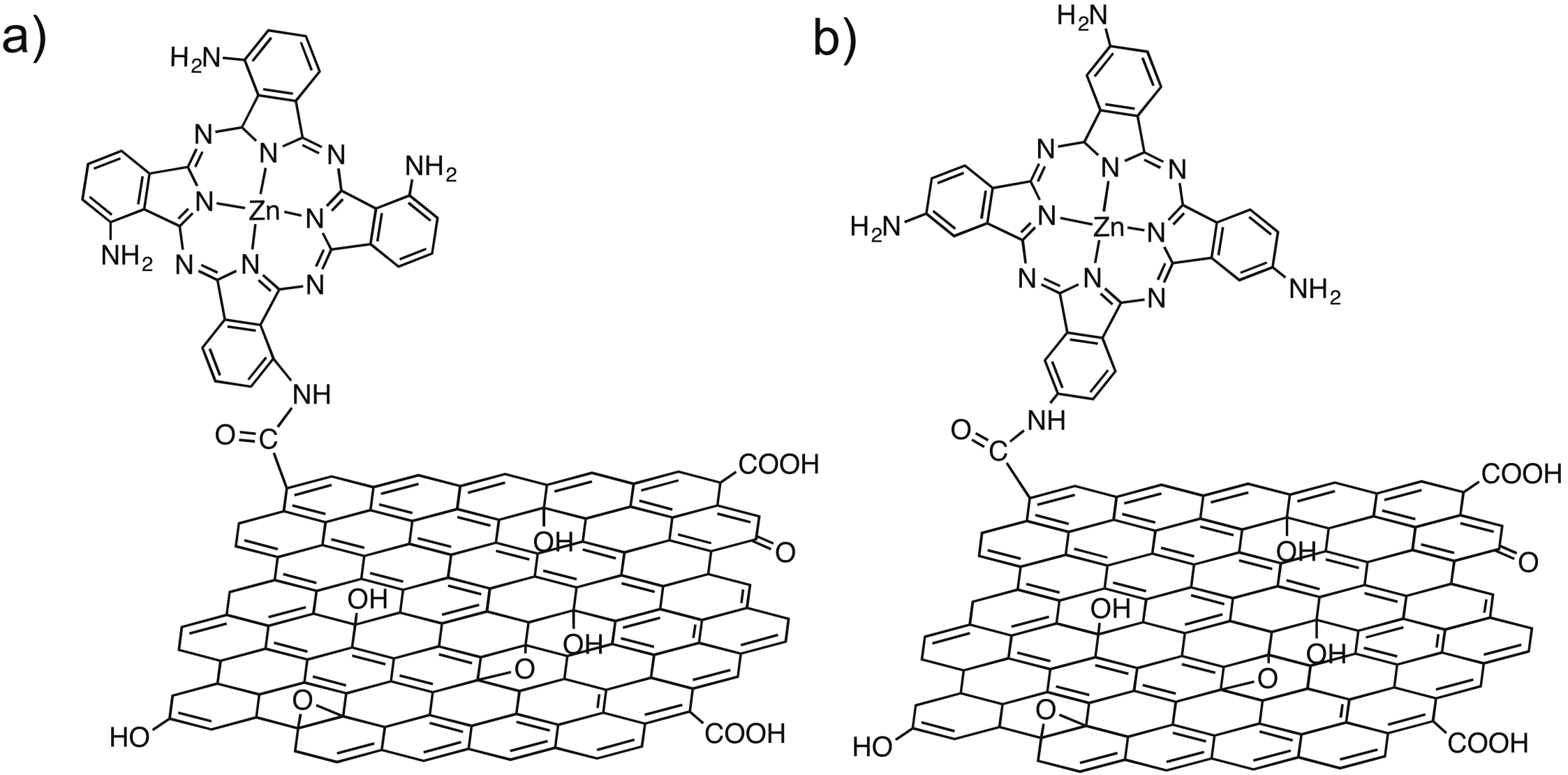
a)
b)
H_2N
NH_2
N
Zn
NH
O=C
COOH
OH
O
HO

a)
b)
Pt
N
NH
O=C
COOH
OH
O
HO
O-
+